Universal spectrum in the infrared range of two-dimensional turbulent flows

Iwayama, Takahiro

Watanabe, Takeshi

(Citation)
Physics of Fluids,26(2):025105-025105

(Issue Date)
2014

(Resource Type)
journal article

(Version)
Version of Record

(URL)
https://hdl.handle.net/20.500.14094/90002599

Universal spectrum in the infrared range of two-dimensional turbulent flows

T. Iwayama and T. Watanabe

Citation: Physics of Fluids (1994-present) **26**, 025105 (2014); doi: 10.1063/1.4864103
View online: http://dx.doi.org/10.1063/1.4864103
View Table of Contents: http://scitation.aip.org/content/aip/journal/pof2/26/2?ver=pdfcov
Published by the AIP Publishing

PHYSICS OF FLUIDS **26**, 025105 (2014)

Universal spectrum in the infrared range of two-dimensional turbulent flows

T. Iwayama[1,a)] and T. Watanabe[2,b)]
[1]*Department of Earth and Planetary Sciences, Graduate School of Science, Kobe University, Kobe 657-8501, Japan*
[2]*Department of Scientific and Engineering Simulation, Graduate School of Engineering, Nagoya Institute of Technology, Gokiso, Showa-ku, Nagoya 466-8555, Japan*

(Received 11 September 2013; accepted 22 January 2014;
published online 10 February 2014)

The low-wavenumber behavior of decaying turbulence governed by the generalized two-dimensional (2D) fluid system, the so-called α-turbulence system, is investigated theoretically and through direct numerical simulation. This system is governed by the nonlinear advection equation for an advected scalar q and is characterized by the relationship between q and the stream function ψ: $q = -(-\nabla^2)^{\alpha/2}\psi$. Here, the parameter α is a real number that does not exceed 3. The enstrophy transfer function in the infrared range ($k \to 0$) is theoretically derived to be $T_\alpha^Q(k \to 0) \sim k^5$ using a quasi-normal Markovianized model of the generalized 2D fluid system. This leads to three canonical cases of the infrared enstrophy spectrum, which depend on the initial conditions: $Q_\alpha(k \to 0) \sim Jk$, $Q_\alpha(k \to 0) \sim Lk^3$, and $Q_\alpha(k \to 0) \sim Ik^5$, where J, L, and I are various integral moments of two-point correlation for q. The prefactors J and L are shown to be invariants of the system, while I is an increasing function of time. The evolution from a narrow initial enstrophy spectrum exhibits a universal infrared enstrophy spectrum of the form $Q_\alpha(k \to 0) \sim k^5$, which is independent of α. These results are verified by direct numerical simulations of the generalized 2D fluid system. © *2014 AIP Publishing LLC*. [http://dx.doi.org/10.1063/1.4864103]

I. INTRODUCTION

The generalized two-dimensional (2D) fluid dynamics, which is governed by the nonlinear advection diffusion equation of the following form:

$$\frac{\partial q}{\partial t} + J(\psi, q) = \mathcal{D} + \mathcal{F}, \tag{1a}$$

$$-(-\nabla^2)^{\alpha/2}\psi = q, \tag{1b}$$

has been actively investigated both theoretically and numerically over the past decade.[1–12] Here, $\psi(\boldsymbol{x}, t)$ is the stream function, $q(\boldsymbol{x}, t)$ is a scalar field advected by the incompressible velocity field $\boldsymbol{v} = \boldsymbol{e}_z \times \nabla\psi$, $\boldsymbol{e}_z$ is a unit vector normal to the plane of motion, J is the 2D Jacobian, α is a real number, ∇^2 is the Laplacian in 2D space, and $\mathcal{D}$ and $\mathcal{F}$ are dissipation and forcing terms, respectively. The generalized 2D fluid system is frequently referred to as the α-turbulence system, because Eq. (1) includes the parameter α and its turbulent properties have been mainly studied up to now. It was originally introduced by Pierrehumbert *et al.*[13] as a tool for studying the effects of spectral non-locality on 2D Navier–Stokes turbulence. It also includes three realizable members of 2D geophysical fluid systems.[13,14] The governing equation given by Eq. (1) reduces to the vorticity

a)iwayama@kobe-u.ac.jp
b)watanabe@nitech.ac.jp

equation for a 2D incompressible barotropic fluid (the 2D Navier–Stokes (NS) system for $\mathcal{D} = \nu\nabla^2 q$, where ν is the kinematic viscosity coefficient, and the 2D Euler system for $\mathcal{D} = 0$) for $\alpha = 2$. Equation (1) is reduced to the governing equation for the surface quasi-geostrophic (SQG) system for $\alpha = 1$.[15,16] The Charney–Hasegawa–Mima (CHM) equation in the asymptotic model (AM) regime[17–19] or the shallow water quasi-geostrophic potential vorticity equation at scales greater than the radius of deformation[20] corresponds to Eq. (1) for $\alpha = -2$.[2,14] Note that for $\alpha > 3$, the azimuthal velocity induced by a point vortex, which is a delta-functional distribution of q, increases with distance, as shown by Iwayama and Watanabe.[9] This calls into question the physical relevance of these systems. Therefore, in the present study, we consider only the case in which $\alpha \leq 3$.

The purpose of investigating the generalized 2D fluid system is generally twofold. The first objective is to understand geophysical 2D fluid systems from a unified perspective. The second is to elucidate the universality and peculiarity of prevailing theories for the 2D Euler and NS systems and further develop them.

Similar to the 2D Euler system, in the absence of dissipation and forcing, Eq. (1) has two quadratic inviscid invariants, the generalized energy $\mathcal{E}_\alpha$ and the generalized enstrophy $\mathcal{Q}_\alpha$:

$$\mathcal{E}_\alpha \equiv -\frac{1}{2}\overline{\psi q}, \tag{2}$$

$$\mathcal{Q}_\alpha \equiv \frac{1}{2}\overline{q^2}, \tag{3}$$

where the overbar denotes the spatial average over the flow domain. For brevity, we herein refer to $\mathcal{E}_\alpha$ and $\mathcal{Q}_\alpha$ as the energy and the enstrophy, respectively. In addition, we refer to q as the generalized vorticity, or simply the vorticity. Note that the vorticity, the energy, and the enstrophy have units of $[q] = L^{2-\alpha}T^{-1}$, $[\mathcal{E}_\alpha] = L^{4-\alpha}T^{-2}$, and $[\mathcal{Q}_\alpha] = L^{4-2\alpha}T^{-2}$, respectively, where L and T are units of length and time, respectively.

Since two inviscid invariants exist, we can infer that cascade phenomena of both invariants in wavenumber space are possible in turbulence governed by Eq. (1), which, for simplicity, is hereinafter referred to as the α-turbulence. Hence, up to now, the turbulent properties of the generalized 2D fluid system have been actively discussed.[1–10,12,13] In particular, efforts were made to analyze the enstrophy spectrum $Q_\alpha(k)$, which is defined as follows:

$$\mathcal{Q}_\alpha \equiv \int_0^\infty Q_\alpha(k)\,\mathrm{d}k, \tag{4}$$

in the enstrophy inertial range of forced and dissipative α-turbulence. The so-called Kraichnan-Leith-Batchelor (KLB) phenomenology[21–23] works well for $\alpha < 2$. However, the enstrophy spectrum in the enstrophy inertial range exhibits a transition at $\alpha = 2$ and deviates from the KLB scaling for $\alpha \geq 2$. In other words, the enstrophy spectrum has the form

$$Q_\alpha(k) \propto \begin{cases} k^{-(7-2\alpha)/3}, & (0 < \alpha < 2), \\ k^{-1}\ln k, & (\alpha = 2), \\ k^{-1}, & (\alpha > 2). \end{cases} \tag{5}$$

This transition of the spectral slope at $\alpha = 2$ is responsible for the dominance of enstrophy transfer by non-local triads compared to that by local triads in the wavenumber space.[4,5,8,13] In contrast, Burgess and Shepherd[12] introduced the eddy damped quasi-normal Markovian (EDQNM) closure for the generalized 2D fluid system and investigated characteristics of self-similar solutions in the energy inertial range of forced and dissipative α-turbulence using the EDQNM closure and numerical simulations. They showed that the KLB phenomenology works well for $\alpha < 5/2$.

Although the inertial range dynamics of forced and dissipative α-turbulence is well understood, our knowledge of the low-wavenumber-range dynamics of decaying α-turbulence is very limited. Here, the low-wavenumber range is defined as wavenumbers k below the wavenumber k_p corresponding to the peak of the energy or enstrophy spectrum, or, alternatively, the centroid wavenumber of the spectrum. The energy spectra in the low-wavenumber range of decaying 2D NS and CHM-AM turbulence have universal slopes.[24–28] For the 2D NS turbulence, Kraichnan[29] first noticed the k^3

dependence of the energy transfer function in the infrared range ($k \to 0$) using the test field model (TFM). Basdevant *et al.*[24] obtained the same result using the EDQNM theory. These studies imply the formation of a k^3 energy spectrum in the infrared range. In contrast, Davidson[27] expanded the energy spectrum in the infrared range as

$$E_2(k) = \frac{Jk^{-1}}{4\pi} + \frac{Lk}{4\pi} + \frac{Ik^3}{16\pi} + \frac{Mk^5}{(4^2)16\pi} + \frac{Nk^7}{(4!)^2 16\pi} + \dots, \tag{6a}$$

where J, L, I, M, and N are expressed in terms of the two-point vorticity correlation, $\langle qq' \rangle \equiv \langle q(\boldsymbol{x})q(\boldsymbol{x}') \rangle$, as follows:

$$J = 2\pi \int_0^\infty r \langle qq' \rangle \, \mathrm{d}r, \tag{6b}$$

$$L = -\frac{\pi}{2} \int_0^\infty r^3 \langle qq' \rangle \, \mathrm{d}r, \tag{6c}$$

$$I = \frac{\pi}{8} \int_0^\infty r^5 \langle qq' \rangle \, \mathrm{d}r, \tag{6d}$$

$$M = -\frac{\pi}{18} \int_0^\infty r^7 \langle qq' \rangle \, \mathrm{d}r, \tag{6e}$$

$$N = \frac{\pi}{32} \int_0^\infty r^9 \langle qq' \rangle \, \mathrm{d}r. \tag{6f}$$

Here, the angle brackets denote the ensemble average, and homogeneity and isotropy are assumed. Then, the correlation function $\langle qq' \rangle$ is a function of the separation $r = |\boldsymbol{r}| = |\boldsymbol{x}' - \boldsymbol{x}|$. Furthermore, Davidson[27] found that the integrals J and L are invariants of freely decaying 2D NS turbulence based on the Kármán-Howarth equation and reported the existence of three canonical cases, $E_2(k \to 0) \sim Jk^{-1}$, $E_2(k \to 0) \sim Lk$, and $E_2(k \to 0) \sim Ik^3$, which depend on the initial condition. For evolution from narrow band initial energy spectra of the form $E_2(k \to 0) \sim k^s$ with $s \geq 3$, which is a traditional set-up for decaying 2D turbulence studies, the energy spectra exhibit the universal form $E_2(k \to 0) \sim k^3$, while the spectra that initially have $E_2(k \to 0) \sim k^{-1}$ or $E_2(k \to 0) \sim k$ preserve their forms in the early stage of evolution but are eventually overshadowed by the k^3 spectrum. These spectra were confirmed by direct numerical simulations.[28,30–32]

For decaying CHM-AM turbulence, Yanase and Yamada[25] first determined that the kinetic energy spectrum $K(k)$, which is defined by

$$\mathcal{K} \equiv \frac{1}{2}\overline{\boldsymbol{v} \cdot \boldsymbol{v}} \equiv \int_0^\infty K(k) \, \mathrm{d}k, \tag{7}$$

has k^7 dependence in the infrared range using a quasi-normal theory. In contrast, Iwayama *et al.*[26] investigated the total energy spectrum in the infrared range of decaying CHM-AM turbulence and obtained a k^5 spectrum using an EDQNM theory. Furthermore, they confirmed the validity of the assumption adopted in the theoretical derivation of the k^5 spectrum and the validity of the predicted spectrum by direct numerical simulations of decaying CHM turbulence. On the other hand, Fox and Davidson[28] reported that the kinetic energy spectrum $K(k)$ for the CHM-AM turbulence has the same form as Eq. (6). Here, the integrals given by Eqs. (6b)–(6f) are expressed in terms of the potential vorticity correlation function in place of the vorticity correlation function. Then, not only J and L, but also I and M, are invariants. Thus, for suitable choices of initial conditions the kinetic energy spectrum exhibits the form $K(k \to 0) \sim k^7$. This was confirmed through direct numerical simulations.[28] Note that the k^5 total energy spectrum is equivalent to the k^7 kinetic energy spectrum. Thus, the above-mentioned results for the infrared range spectrum for decaying CHM-AM turbulence are consistent with each other.

On the other hand, Tran and Dritschel[33] discussed the large-scale dynamics by considering the evolution of a dynamical quantity characterizing the large-scale behavior of the SQG and 2D Euler flows. They derived upper bounds for the evolution of the modal stream function for the SQG and Euler flows using the Cauchy-Schwarz inequality. Their results imply that the kinetic energy spectra at small wavenumbers scale like k^3 and k^5 for the Euler and SQG flows, respectively. However, the result for the SQG case has not been verified by numerical simulations yet.

Although the infrared spectra of decaying 2D turbulence for three of the members of the generalized 2D fluid system have been investigated as mentioned above, those for arbitrary α have not yet been investigated. The infrared range dynamics is of fundamental importance because this range may carry a significant part of the energy and enstrophy, and the infrared range dynamics involves the existence of integral invariants for decaying turbulence and the existence of a universal spectral form for the initial narrow-band spectrum. Therefore, we theoretically derive the infrared enstrophy spectrum of decaying α-turbulence in the present study.

For theoretical analysis of the enstrophy spectrum in the infrared range, we follow the study of Basdevant *et al.*[24] (henceforth BLS78). They derived the infrared energy spectrum of 2D NS turbulence using the EDQNM closure theory. Their method was also used by Iwayama *et al.*[26] in the derivation of the total energy spectrum in the infrared range of decaying CHM-AM turbulence. There are another two methods for the derivation of the infrared spectrum based on the TFM[29] and the Kármán-Howarth equation.[27] The EDQNM closure theory and the TFM are constructed by equations in Fourier space while the Kármán–Howarth equation is written in terms of physical space quantities. Since the fractional Laplacian operator $(-\nabla^2)^{\alpha/2}$ is defined as k^α by a Fourier transform, the EDQNM closure theory and the TFM are more useful methods for the derivation of the infrared spectrum of the present system than the Kármán–Howarth equation. Moreover, the EDQNM closure for the generalized 2D fluid system was introduced by Burgess and Shepherd,[12] whereas the TFM for the present system has not yet been obtained. Furthermore, the EDQNM closure is the most common and easiest closure for handling. Therefore, we use the EDQNM closure in the present study.

The significance of the present study does not lie in a geophysical side but a pure physical side, although the purpose of investigating the generalized 2D fluid system is generally twofold as we mentioned. It is well known that the planetary rotation plays a significant role for dynamics of geophysical flows. The planetary rotation causes the propagation of the Rossby waves and makes the flow structure anisotropic.[34] However, a term representing the planetary rotation, the so-called beta term, is excluded in Eq. (1). Furthermore, since the planetary rotation affects large scales, the infrared range would not be in the turbulent regime but in the wave regime where the Rossby waves play a significant role. In this sense, the present study aims to purely physical interest.

The remainder of the present paper is organized as follows. In Sec. II, we briefly introduce a quasi-normal Markovian model of the generalized 2D fluid system. In Sec. III, we derive the power-law exponent of the enstrophy spectrum in the infrared range of decaying α-turbulence using the method proposed by BLS78. In Sec. IV, we present the results obtained from direct numerical simulations of Eq. (1). In Sec. V, we show that the prevailing infrared spectra for the 2D NS, CHM-AM, and SQG turbulence are included as special cases of the theoretical results of the present study. Furthermore, the self-similarity of the enstrophy spectrum obtained in Sec. IV is examined. Finally, we summarize the results in Sec. VI.

II. FORMULATION

A. Spectral form and enstrophy equation of the generalized 2D fluid system

We consider a system that is confined within the square domain of side length L with periodic boundary conditions. Furthermore, we set the damping term $\mathcal{D}$ of Eq. (1a) as a hyperviscosity term

$$\mathcal{D} = -\nu_p(-\nabla^2)^p q, \tag{8}$$

and the forcing term $\mathcal{F}$ being zero. We then expand the stream function and the vorticity in a Fourier series:

$$\psi(\boldsymbol{x}) = \sum_{\boldsymbol{k}} \hat{\psi}(\boldsymbol{k}) \exp(i\boldsymbol{k}\cdot\boldsymbol{x}), \tag{9}$$

$$q(\boldsymbol{x}) = \sum_{\boldsymbol{k}} \hat{q}(\boldsymbol{k}) \exp(i\boldsymbol{k}\cdot\boldsymbol{x}), \tag{10}$$

respectively, where $\boldsymbol{k} = 2\pi\boldsymbol{n}/L$ is the wave vector and the summation is taken over the integer vector $\boldsymbol{n} = (n_x, n_y)$. Substituting Eqs. (9) and (10) into Eq. (1) yields the Fourier space version of the governing equation:

$$\left(\frac{\partial}{\partial t} + \nu_p k^{2p}\right)\hat{q}(\boldsymbol{k}) = \sum_{\boldsymbol{l}}\sum_{\boldsymbol{m}} \delta_{\boldsymbol{k}+\boldsymbol{l}+\boldsymbol{m},\boldsymbol{0}} \frac{\boldsymbol{e}_z\cdot(\boldsymbol{l}\times\boldsymbol{m})(l^\alpha - m^\alpha)}{2l^\alpha m^\alpha}\hat{q}^*(\boldsymbol{l})\hat{q}^*(\boldsymbol{m}), \tag{11a}$$

$$\hat{q}(\boldsymbol{k}) = -k^\alpha \hat{\psi}(\boldsymbol{k}). \tag{11b}$$

Here $k = |\boldsymbol{k}|$, $l = |\boldsymbol{l}|$, and $m = |\boldsymbol{m}|$. The asterisk denotes the complex conjugate. For brevity, the time argument is omitted. The temporal evolution of the enstrophy spectrum $Q_\alpha(k)$, which is defined as follows:

$$\mathcal{Q}_\alpha = \sum_k Q_\alpha(k), \tag{12a}$$

$$Q_\alpha(k) = \sum_{|\boldsymbol{k}'|=k}^{\text{shell}} \frac{1}{2}\left\langle |\hat{q}(\boldsymbol{k}')|^2 \right\rangle, \tag{12b}$$

is governed by

$$\left(\frac{\partial}{\partial t} + 2\nu_p k^{2p}\right) Q_\alpha(k) = T_\alpha^{\mathcal{Q}}(k), \tag{13}$$

where $\sum_{|\boldsymbol{k}'|=k}^{\text{shell}}$ is the shell summation in $k - \frac{\Delta k}{2} \le |\boldsymbol{k}'| < k + \frac{\Delta k}{2}$, $\Delta k = 2\pi/L$, and $T_\alpha^{\mathcal{Q}}(k)$ is the enstrophy transfer function. The enstrophy transfer function $T_\alpha^{\mathcal{Q}}(k)$ can be expressed in terms of the triad enstrophy transfer function $T_\alpha^{\mathcal{Q}}(k,l,m)$ as follows:

$$T_\alpha^{\mathcal{Q}}(k) = \sum_{l,m} \frac{1}{2} T_\alpha^{\mathcal{Q}}(k,l,m), \tag{14a}$$

$$T_\alpha^{\mathcal{Q}}(k,l,m) = \sum_{|\boldsymbol{k}'|=k}^{\text{shell}} \sum_{|\boldsymbol{l}'|=l}^{\text{shell}} \sum_{|\boldsymbol{m}'|=m}^{\text{shell}} \frac{\boldsymbol{e}_z\cdot(\boldsymbol{l}'\times\boldsymbol{m}')(l'^\alpha - m'^\alpha)}{l'^\alpha m'^\alpha} \Re\mathfrak{e}\left[\left\langle \hat{q}(\boldsymbol{k}')\hat{q}(\boldsymbol{l}')\hat{q}(\boldsymbol{m}')\right\rangle\right] \delta_{\boldsymbol{k}'+\boldsymbol{l}'+\boldsymbol{m}',\boldsymbol{0}}. \tag{14b}$$

Here, $\Re\mathfrak{e}[\bullet]$ denotes the real part of a complex number. Since $T_\alpha^{\mathcal{Q}}(k,l,m)$ satisfies a detailed balance $T_\alpha^{\mathcal{Q}}(k,l,m) + T_\alpha^{\mathcal{Q}}(l,m,k) + T_\alpha^{\mathcal{Q}}(m,k,l) = 0$, for wavenumbers that form the triangle $\boldsymbol{k}+\boldsymbol{l}+\boldsymbol{m} = \boldsymbol{0}$, and is symmetric with respect to l and m, i.e., $T_\alpha^{\mathcal{Q}}(k,l,m) = T_\alpha^{\mathcal{Q}}(k,m,l)$, the enstrophy flux

$$\Pi_\alpha^{\mathcal{Q}}(k) = \sum_{k'>k} T_\alpha^{\mathcal{Q}}(k') \tag{15}$$

can be divided into two parts:[35]

$$\Pi_\alpha^{\mathcal{Q}}(k) = \Pi_\alpha^{\mathcal{Q}^{(+)}}(k) - \Pi_\alpha^{\mathcal{Q}^{(-)}}(k), \tag{16a}$$

$$\Pi_\alpha^{\mathcal{Q}(+)}(k) = \sum_{k'>k} \sum_{l<k} \sum_{m<l} T_\alpha^{\mathcal{Q}}(k', l, m), \tag{16b}$$

$$\Pi_\alpha^{\mathcal{Q}(-)}(k) = \sum_{k'<k} \sum_{l>k} \sum_{k<m<l} T_\alpha^{\mathcal{Q}}(k', l, m). \tag{16c}$$

Here, $\Pi_\alpha^{\mathcal{Q}(+)}(k)$ is the net enstrophy input into all wavenumbers $>k$ from interactions with l and m, which are both $<k$, whereas $\Pi_\alpha^{\mathcal{Q}(-)}(k)$ is the net enstrophy input into all wavenumbers $<k$ from interactions with l and m, which are both $>k$.

B. A quasi-normal Markovian model of the α-turbulence equation

In the limit $L \to \infty$, Eqs. (12a), (14a), (15), (16b), and (16c) are represented in terms of integrals, i.e.,

$$\mathcal{Q}_\alpha = \int_0^\infty Q_\alpha(k)\, \mathrm{d}k, \tag{17}$$

$$T_\alpha^{\mathcal{Q}}(k) = \frac{1}{2} \int_0^\infty \int_0^\infty T_\alpha^{\mathcal{Q}}(k, l, m)\, \mathrm{d}l\, \mathrm{d}m, \tag{18}$$

$$\Pi_\alpha^{\mathcal{Q}}(k) = \int_k^\infty T_\alpha^{\mathcal{Q}}(k')\, \mathrm{d}k', \tag{19}$$

$$\Pi_\alpha^{\mathcal{Q}(+)}(k) = \int_k^\infty \mathrm{d}k' \int_0^k \mathrm{d}l \int_0^l \mathrm{d}m\, T_\alpha^{\mathcal{Q}}(k', l, m), \tag{20}$$

$$\Pi_\alpha^{\mathcal{Q}(-)}(k) = \int_0^k \mathrm{d}k' \int_k^\infty \mathrm{d}l \int_k^l \mathrm{d}m\, T_\alpha^{\mathcal{Q}}(k', l, m). \tag{21}$$

Using a quasi-normal Markovian approximation,[12,36] Eq. (14b) is reduced to

$$T_\alpha^{\mathcal{Q}}(k, l, m) = \frac{2k^{\alpha+2}}{\pi lm}\, \theta_{klm} \left[2a_{klm}\, \frac{k}{(lm)^\alpha}\, Q_\alpha(l)\, Q_\alpha(m) - b_{klm} \frac{l}{(mk)^\alpha}\, Q_\alpha(m)\, Q_\alpha(k) - b_{kml}\, \frac{m}{(kl)^\alpha}\, Q_\alpha(k)\, Q_\alpha(l) \right], \tag{22}$$

where $T_\alpha^{\mathcal{Q}}(k, l, m) = 0$ outside of the domain in the (l, m) plane such that k, l, and m can be the sides of the triangle $\boldsymbol{k} = \boldsymbol{l} + \boldsymbol{m}$ (Fig. 1), and

$$a_{klm} = \frac{b_{klm} + b_{kml}}{2}, \tag{23a}$$

$$b_{klm} = 2\, \frac{(l^\alpha - m^\alpha)(k^\alpha - m^\alpha)\sqrt{1 - x^2}}{k^{\alpha+2}(lm)^{\alpha-2}}, \tag{23b}$$

$$b_{kml} = 2\, \frac{(m^\alpha - l^\alpha)(k^\alpha - l^\alpha)\sqrt{1 - x^2}}{k^{\alpha+2}(lm)^{\alpha-2}}, \tag{23c}$$

are the geometric coefficients, and x refers to the cosine of the interior angle of the triangle facing the side k, i.e.,

$$x = \frac{\boldsymbol{l} \cdot \boldsymbol{m}}{lm}. \tag{24}$$

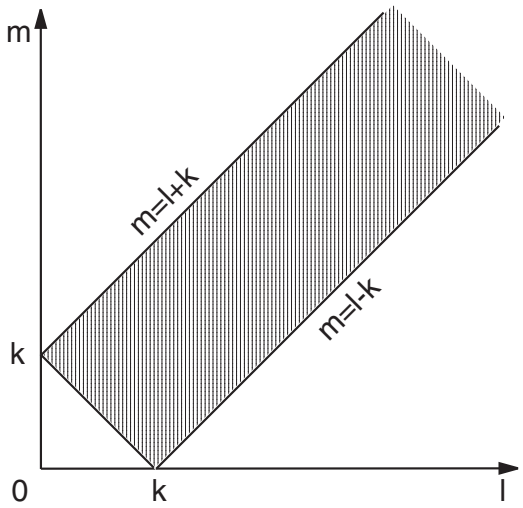

FIG. 1. Domain in the (l, m) plane such that k, l, and m can be the sides of the triangle $\boldsymbol{k} = \boldsymbol{l} + \boldsymbol{m}$. The triad enstrophy transfer function $T_\alpha^Q(k, l, m)$ has a non-zero value within the hatched region.

The function θ_{klm} is the relaxation time of the third-order moments associated with the triad (k, l, m), the functional form of which is different for different theories. There is an approximation that introduces eddy damping effects in θ_{klm}, referred to as the EDQNM.[36] In this approximation, θ_{klm} is expressed as follows:

$$\theta_{klm} = \frac{1}{\mu_{klm}}, \tag{25a}$$

$$\mu_{klm} = \mu_k + \mu_l + \mu_m, \tag{25b}$$

$$\mu_k = \mu \left[k^{5-2\alpha} Q_\alpha(k)\right]^{1/2}. \tag{25c}$$

Equation (25c) is derived by Eqs. (2.4) and (5.8) in Burgess and Shepherd[12] and using the relation

$$Q_\alpha(k) = k^\alpha E_\alpha(k). \tag{26}$$

The proportionality constant μ in Eq. (25c) has not yet been determined. However, as shown in Sec. III, the power-law exponent of the enstrophy spectrum in the infrared range is independent of μ. Thus, the concrete value of μ is unnecessary in the present study. Note that usual closure equations are written in terms of the energy spectrum. However, we express the enstrophy transfer function in terms of the enstrophy spectrum, because the purpose of the present study is to derive the enstrophy spectrum in the infrared range.

Equations (12b) and (14)–(16) are used in the analysis of the direct numerical simulations of Eq. (1), whereas Eqs. (18)–(23) are used in the theoretical derivation of the enstrophy spectrum in the infrared range of α-turbulence.

III. DERIVATION OF THE ENSTROPHY SPECTRUM IN THE INFRARED RANGE OF DECAYING α-TURBULENCE

In this section, we derive the enstrophy spectrum in the infrared range of decaying α-turbulence using the method proposed by BLS78.[24]

The method proposed by BLS78[24] is summarized as follows:[26,36]

1. Interactions among triad wave vectors $\boldsymbol{k}$, $\boldsymbol{l}$, and $\boldsymbol{m}$ can be divided into two categories: (1) either all of $\boldsymbol{k}$, $\boldsymbol{l}$, and $\boldsymbol{m}$ have comparable magnitude, or (2) one of $\boldsymbol{k}$, $\boldsymbol{l}$, and $\boldsymbol{m}$ is very small in comparison with the others. The former refers to the local interactions, and the latter refers to the non-local interactions. The enstrophy transfer function $T_\alpha^{\mathcal{Q}}(k)$ can then be divided into two parts: $T_{\alpha\,\mathrm{L}}^{\mathcal{Q}}(k)$ constructed from the local triad interactions, and $T_{\alpha\,\mathrm{NL}}^{\mathcal{Q}}(k)$ from the non-local triad interactions.
2. Assume that the non-local triad interactions with elongated triads $k \ll l \simeq m$ are dominant in the infrared range. Then, one introduces the small parameter ϵ, which is the ratio of two interacting wavenumbers, $\epsilon \equiv k/l$, and expresses $T_{\alpha\,\mathrm{NL}}^{\mathcal{Q}}(k)$ in terms of power series in ϵ.
3. Practical calculation is performed through the enstrophy flux $\Pi_\alpha^{\mathcal{Q}}(k)$. Instead of calculating the enstrophy transfer function $T_{\alpha\,\mathrm{NL}}^{\mathcal{Q}}(k)$ directly, we evaluate the non-local part of the energy flux $-\Pi_{\alpha\,\mathrm{NL}}^{\mathcal{Q}(-)}(k)$, which is equivalent to $\Pi_{\alpha\,\mathrm{NL}}^{\mathcal{Q}}(k)$ because the elongated triads $k \ll l \simeq m$ cannot contribute to the flux $\Pi_\alpha^{\mathcal{Q}(+)}(k)$. In other words, $\Pi_{\alpha\,\mathrm{NL}}^{\mathcal{Q}(+)}(k)$ is geometrically forbidden. Differentiating the resulting enstrophy flux with respect to wavenumber, the non-local part of the enstrophy transfer function is recovered. Then, the wavenumber dependence of the enstrophy transfer function gives the functional form of the enstrophy spectrum in the infrared range.

Following the above method, we derive the enstrophy spectrum in the infrared range of decaying α-turbulence. The non-local part of $\Pi_\alpha^{\mathcal{Q}(-)}(k)$ is given by

$$\Pi_{\alpha\,\mathrm{NL}}^{\mathcal{Q}(-)}(k) \equiv \int_0^k \mathrm{d}k' \int_{sup(k,k'/\epsilon)}^{\infty} \mathrm{d}l \int_{l-k'}^{l} \mathrm{d}m\, T_\alpha^{\mathcal{Q}}(k', l, m), \tag{27}$$

where $\epsilon = k'/l$ and the lower limit on the m integral is a geometrical constraint. Using the cosine law:

$$m^2 = k'^2 + l^2 - 2k'lz, \tag{28}$$

where z is the cosine of the interior angle of the triangle $\boldsymbol{k}' = \boldsymbol{l} + \boldsymbol{m}$ facing the side m, i.e.,

$$z = \frac{\boldsymbol{k}' \cdot \boldsymbol{l}}{k'l}, \tag{29}$$

we transform the variable m in Eq. (27) to z. Then, Eq. (27) is rewritten as

$$\Pi_{\alpha\,\mathrm{NL}}^{\mathcal{Q}(-)}(k) = \int_0^k \mathrm{d}k' \int_{sup(k,k'/\epsilon)}^{\infty} \mathrm{d}l \int_{k'/(2l)}^{1} \mathrm{d}z\, \frac{k'l}{m}\, T_\alpha^{\mathcal{Q}}(k', l, z). \tag{30}$$

Next, we expand the integrand in Eq. (30) with respect to the smallness parameter ϵ. The calculation of the expansion is described in detail in Appendix A. To the leading order in ϵ, the detailed enstrophy transfer function $T_\alpha^{\mathcal{Q}}(k', l, z)$ is expressed as

$$\begin{aligned} T_\alpha^{\mathcal{Q}}(k', l, z) \simeq \frac{4z^2\sqrt{1-z^2}}{\pi}\theta_{k'll}\Big[&\alpha^2 l^{-(2\alpha+1)}\{Q_\alpha(l)\}^2 k'^4 \\ &-\alpha l^{-\alpha}\left\{\frac{\partial\{l\,Q_\alpha(l)\}}{\partial l} - 2Q_\alpha(l)\right\} k'^{3-\alpha} Q_\alpha(k') H(\alpha) \\ &+\alpha l^{-2\alpha}\left\{\frac{\partial\{l\,Q_\alpha(l)\}}{\partial l} - (\alpha+2)Q_\alpha(l)\right\} k'^3 Q_\alpha(k') H(-\alpha)\Big]. \end{aligned} \tag{31}$$

Here, $H(x)$ is the Heaviside step function. Inserting Eq. (31) into Eq. (30), taking the integral with respect to z, and differentiating the resulting equation with respect to k, we finally obtain

$$T_{\alpha\ \mathrm{NL}}^{\mathcal{Q}(-)}(k) = \frac{\partial \Pi_{\alpha\ \mathrm{NL}}^{\mathcal{Q}(-)}(k)}{\partial k}$$
$$\simeq \frac{\alpha^2}{4}\left[\int_{k/\epsilon}^{\infty} \theta_{kll}\, l^{-(2\alpha+1)}\{Q_\alpha(l)\}^2\,\mathrm{d}l\right] k^5 - 2\nu_{\mathrm{T}}^{(+)}(k)k^{4-\alpha}\,Q_\alpha(k)H(\alpha)$$
$$- 2\nu_{\mathrm{T}}^{(-)}(k)k^4\,Q_\alpha(k)H(-\alpha), \tag{32a}$$

where

$$\nu_{\mathrm{T}}^{(+)}(k) \equiv \frac{\alpha}{8}\int_{k/\epsilon}^{\infty} \theta_{kll}\, l^{-\alpha}\left[\frac{\partial\{l\,Q_\alpha(l)\}}{\partial l} - 2Q_\alpha(l)\right]\mathrm{d}l, \tag{32b}$$

$$\nu_{\mathrm{T}}^{(-)}(k) \equiv \frac{|\alpha|}{8}\int_{k/\epsilon}^{\infty} \theta_{kll}\, l^{-2\alpha}\left[\frac{\partial\,\{l\,Q_\alpha(l)\}}{\partial l} - (\alpha+2)Q_\alpha(l)\right]\mathrm{d}l. \tag{32c}$$

Here, in the integral with respect to z, we have used

$$\int_{2k'/l}^{1} z^2\sqrt{1-z^2}\,\mathrm{d}z \simeq \int_0^1 z^2\sqrt{1-z^2}\,\mathrm{d}z = \frac{\pi}{16}. \tag{33}$$

The quantities $\nu_{\mathrm{T}}^{(+)}(k)$ and $\nu_{\mathrm{T}}^{(-)}(k)$ are the α-turbulence version of the eddy viscosity derived by Kraichnan for the 2D NS equation.[29] As mentioned in Appendix A, the first and second term of the eddy viscosity term are negligible when $\alpha < 0$ and $\alpha > 0$, respectively.

The second and third terms on the right-hand side of Eq. (32a) are negligible in the infrared range, because $Q_\alpha(k) \to 0$ in the limit $k \to 0$ for decaying turbulence. Moreover, the viscous damping term, i.e., the second term on the left-hand side of Eq. (13), is also negligible in the infrared range. Then, Eq. (13) is reduced to

$$\frac{\partial\, Q_\alpha(k)}{\partial t} \simeq \frac{\alpha^2}{4}\left[\int_{k/\epsilon}^{\infty} l^{-(2\alpha+1)}\theta_{kll}\{Q_\alpha(l)\}^2\,\mathrm{d}l\right]k^5. \tag{34}$$

Here, the integral in Eq. (32a) would be nearly independent of its lower limit because the integral is dominated by the energy containing scales.

On the other hand, the enstrophy spectrum $Q_\alpha(k)$ is expressed in terms of the Hankel transform of the vorticity correlation function as

$$Q_\alpha(k) = \frac{1}{2}\int_0^\infty \langle qq'\rangle kr\, J_0(kr)\,\mathrm{d}r. \tag{35}$$

Here, we assumed the homogeneity and isotropy of the vorticity field. Furthermore, $J_0(x)$ is a Bessel function of the first kind of order zero. (Note that the Bessel function formulae required for the present study are listed in Appendix B.) Then, the enstrophy spectrum can be expressed in terms of series expansion in wavenumber space as

$$Q_\alpha(k) = \frac{Jk}{4\pi} + \frac{Lk^3}{4\pi} + \frac{Ik^5}{16\pi} + \ldots. \tag{36}$$

The prefactors J, L, and I are defined by Eqs. (6b), (6c), and (6d), respectively. Inserting Eq. (36) into Eq. (34), we obtain

$$\left\{\frac{k}{4\pi}\frac{\mathrm{d}J}{\mathrm{d}t} + \frac{k^3}{4\pi}\frac{\mathrm{d}L}{\mathrm{d}t} + \frac{k^5}{16\pi}\frac{\mathrm{d}I}{\mathrm{d}t} + \ldots\right\} \simeq \frac{\alpha^2}{4}\left[\int_{k/\epsilon}^{\infty} l^{-(2\alpha+1)}\theta_{kll}\{Q_\alpha(l)\}^2\,\mathrm{d}l\right]k^5. \tag{37}$$

Hence, Eq. (37) indicates that both J and L are invariants of the present system. In contrast, I is not an invariant, but rather an increasing function of time, because the right-hand side of Eq. (37) is

positive definite. Furthermore, Eq. (37) indicates that, for the initial enstrophy spectrum with $J = L = 0$, the infrared enstrophy spectrum takes the form

$$Q_\alpha(k \to 0) \sim k^5. \tag{38}$$

On the other hand, the enstrophy spectra starting as $Q_\alpha(k \to 0) \sim Jk$ or $Q_\alpha(k \to 0) \sim Lk^3$ must remain in these forms but are eventually overshadowed by the Ik^5 spectrum from the high-wavenumber side.

We will compare the above result with the prevailing infrared spectra for the 2D NS, CHM-AM, and SQG turbulence in Sec. V. In Sec. IV, we perform direct numerical simulations of decaying α-turbulence, and the resulting enstrophy spectra and enstrophy transfers are examined.

IV. NUMERICAL SIMULATIONS

A. Overview of the simulations

In this section, we report direct numerical simulations of decaying turbulence governed by Eq. (11) with the normal viscosity $p = 1$. First, we outline the numerical method, the initial conditions used, and the resolution of the calculations.

The pseudo-spectral method is used in double-precision arithmetic at a resolution of N^2, which is the number of grid points in the computational domain $[0, L]^2$, and the truncation wavenumber k_T is taken according to the two-third dealiasing technique or the phase shift technique.[37] In order to ensure the extent of the low-k region of the spectrum, we adopt the domain size as $L = 8\pi$. We set $N = 4096$, meaning that the minimum grid point size is equivalent to $N = 1024$ resolution simulation with the standard domain size $L = 2\pi$, while the increment of the wavenumber is $\Delta k = 0.25$. Then, $k_\mathrm{T} = 341$ for the two-third dealiasing technique, and $k_\mathrm{T} = 482$ for the phase shift technique.

Time integration is performed by the second-order Adams-Bashforth scheme with a variable time step, and the viscous term is calculated implicitly using an integrating factor. The next step of $\hat{q}(\boldsymbol{k}, t)$ is then calculated according to

$$\hat{q}(\boldsymbol{k}, t + \Delta t) = e^{-\nu_p k^{2p} \Delta t} \hat{q}(\boldsymbol{k}, t) + \frac{1}{2} \Delta t \, e^{-\nu_p k^{2p} \Delta t} \left\{ 3\hat{\mathcal{N}}(\boldsymbol{k}, t) - e^{-\nu_p k^{2p} \Delta t} \hat{\mathcal{N}}(\boldsymbol{k}, t - \Delta t) \right\}, \tag{39}$$

where $\hat{\mathcal{N}}$ stands for the right-hand side of Eq. (11a). The increment of time Δt is determined by the Courant–Friedrich-Lewy condition:

$$\Delta t = C \frac{L/N}{\max [|\boldsymbol{v}|]}, \tag{40}$$

where max [•] indicates the maximum value attained over all of the grid points. We set the Courant number as $C = 0.1$. As preliminary calculations, we performed simulations with $N = 1024$ and $L = 2\pi$ with the fourth-order Runge-Kutta scheme for time integration in the case of $\alpha = 1$ and $\alpha = 2$. We confirmed that the results are independent of the time integration scheme. Thus, we adopt the Adams-Bashforth scheme in the present study for computational efficiency.

Initial conditions are made by generating uniform random numbers with values between 0 and 2π for the phase of each Fourier component of q. We normalize the initial value of the energy per unit area to be 0.1, and the initial form of the enstrophy spectrum has the form

$$Q_\alpha(k) \propto k^s \exp\left[-\frac{|s|}{2} \left(\frac{k}{k_\mathrm{p}} \right)^2 \right], \tag{41}$$

where $k_\mathrm{p} = 50$ and $s = 1, 3, 5$, and 7. These initial conditions are the same as those used in previous studies.[28,31,32,38] Ensembles of eight runs are performed for all cases in order to improve the statistical convergence of the results.

We define the Reynolds number as follows:

$$Re \equiv \frac{\sqrt{2\mathcal{K}}\ell}{\nu_1}, \tag{42}$$

TABLE I. Parameters for numerical simulations.

α	s	$\mathcal{Q}_\alpha(0)$	$\mathcal{K}(0)$	$k_\mathrm{d}(0)$	$\omega_0(0)$	$\ell_q(0)$	k_T
1	1	3.999	3.999	531.8	200.0	2.505×10^{-2}	482
1	3	4.607	4.607	515.7	175.2	2.171×10^{-2}	482
1	5	4.758	4.758	510.5	169.0	2.102×10^{-2}	482
1	7	4.825	4.825	507.9	166.0	2.073×10^{-2}	482
2	1	43.34	0.1	145.3	9.311	2.505×10^{-2}	482
2	3	166.7	0.1	212.7	18.26	2.171×10^{-2}	482
2	5	200.0	0.1	222.1	20.00	2.102×10^{-2}	482
2	7	214.3	0.1	225.4	20.70	2.073×10^{-2}	482
3	1	43.66	2.680×10^{-1}	28.77	0.4488	2.505×10^{-2}	341
3	3	3855	1.449×10^{-2}	100.2	2.151	2.171×10^{-2}	482
3	5	7136	3.568×10^{-3}	133.9	2.671	2.102×10^{-2}	482
3	7	8616	2.815×10^{-3}	142.6	2.836	2.073×10^{-2}	482

where ℓ is an integral scale that is defined by $\ell \equiv (\mathcal{E}_\alpha/\mathcal{Q}_\alpha)^{1/\alpha}$. This is a natural extension of the Reynolds number used in previous studies.[31,32,38] Furthermore, we define the enstrophy dissipation wavenumber k_d as

$$k_\mathrm{d} \equiv \left(\frac{\eta}{\nu_p^3}\right)^{1/\{2(\alpha+3p-2)\}}, \tag{43}$$

where η is the enstrophy dissipation rate.

All of the simulations are performed with $Re(t=0) = 100$. This is the similar initial Reynolds numbers in the previous studies on the infrared spectrum.[28,32] (Note that although the definition of the Reynolds number used by Fox and Davidson[28] is different from the present study, the values of their Reynolds numbers are comparable with those of ours.) Although the highest Reynolods numbers used in Fox and Davidson[28] was $Re = 200$, most of their simulations were performed with $Re = 100$. Ossia and Lesieur[32] was performed with $Re = 6.64$ and 131. In both papers, hyperviscosity simulations were also conducted and they showed that there is little difference of the slope of the infrared spectrum between the normal viscosity and hyperviscosity simulations. The initial large eddy-turnover time is taken as $1/\omega_0$, where $\omega_0 \equiv \sqrt{2\mathcal{Q}_2}$. All numerical simulations are performed up to approximately 1700, 200, and 20 initial turnover times for $\alpha = 1, 2$, and 3, respectively. The details of the simulations are tabulated in Table I. Although the initial dissipation wavenumbers $k_\mathrm{d}(0)$ slightly exceeded k_T for $\alpha = 1$, we checked that k_d quickly decayed in the early stage of evolution and the dissipation ranges were well resolved during almost all the simulation period.

B. Results

First, we examine the evolution of global quantities, the energy, the enstrophy, the Reynolds number, and an integral scale of the vorticity field. The temporal evolution of the energy is shown in Fig. 2. Although the energy is an inviscid invariant, the energy gradually decays with time due to the finiteness of the Reynolds number. We concentrate on the dependence of the decay of energy on s when the value of α is fixed. The energy for $s = 1$ decreases much more slowly than the energies for $s = 3, 5$, and 7. The initial energy spectrum for $s = 1$ has the form $E_\alpha(k) \sim k^{1-\alpha}$ in the lower wavenumber range, which indicates that a large proportion of the energy is concentrated in the lower-wavenumber range. Thus, the dissipation of energy is less effective for $s = 1$. There is little difference among the decays of energy for $s = 3, 5$, and 7. In particular, the decays of energy for $s = 5$ and $s = 7$ are quite similar.

The temporal evolution of the enstrophy is shown in Fig. 3. The enstrophy decays much faster than the energy. Since the enstrophy is a higher wavenumber weighted quantity than the energy for $\alpha > 0$, the dissipation effect is more efficient for the enstrophy than the energy. As before, we

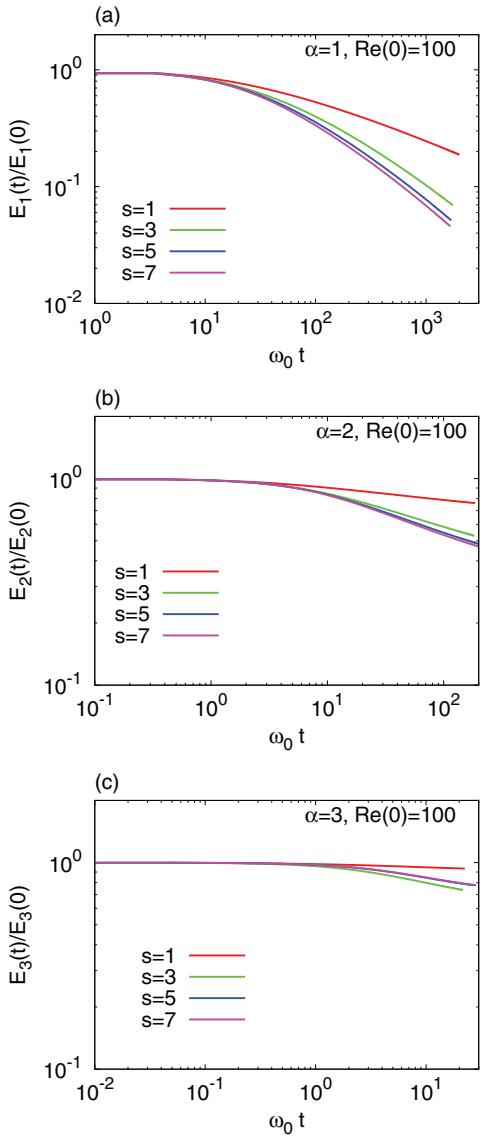

FIG. 2. Time evolution of energy normalized by the initial value, $\mathcal{E}_\alpha(t)/\mathcal{E}_\alpha(0)$, for (a) $\alpha = 1$, (b) $\alpha = 2$, and (c) $\alpha = 3$. The red, green, blue, and violet lines indicate the evolutions for $s = 1, 3, 5$, and 7, respectively.

concentrate on the dependence of the decay of enstrophy on s as the value of α is fixed. After the initial faster decay stage, the enstrophy for $s = 1$ decays more slowly than that for $s = 3, 5$, and 7. There is little difference between the algebraic decay of enstrophy for $s = 3, 5$, and 7. In particular, the decay of enstrophy for $s = 5$ and $s = 7$ are quite similar.

The temporal evolution of the Reynolds number, as defined by Eq. (42), is shown in Fig. 4. For $\alpha = 1$ starting with $s = 1$, the Reynolds number increases with time. In contrast, for $\alpha = 1$ with $s = 3, 5$, and 7, the Reynolds number decreases slightly. Based on numerical simulations of decaying 2D NS turbulence with a narrow initial energy spectrum, Chasnov[31] found a critical initial Reynolds number Re_c, such that, for $Re(0) < Re_c$, the Reynolds number decays monotonically with time and, for $Re(0) > Re_c$, the Reynolds number decreases initially and then increases asymptotically. Through numerical simulations, Chasnov demonstrated that $Re_c \approx 15.73$. At $Re(0) = Re_c$, the energy and the enstrophy decay as $\mathcal{E}_2 \sim t^{-1}$ and $\mathcal{Q}_2 \sim t^{-2}$, respectively, and the energy spectrum exhibits self-similar evolution. Since the present numerical simulations were performed at $Re(0) = 100$, the

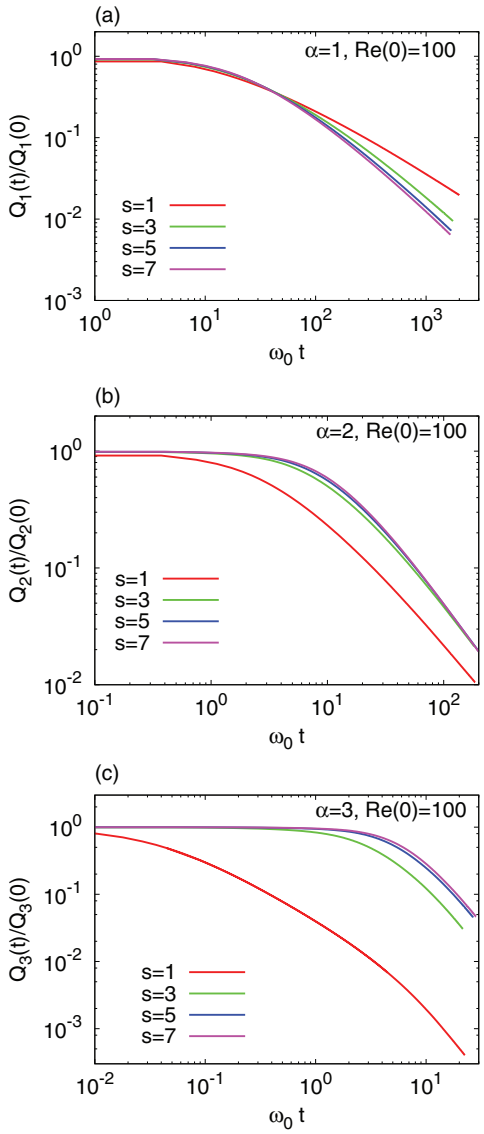

FIG. 3. Time evolution of enstrophy normalized by the initial value, $\mathcal{Q}_\alpha(t)/\mathcal{Q}_\alpha(0)$, for (a) $\alpha = 1$, (b) $\alpha = 2$, and (c) $\alpha = 3$. The red, green, blue, and violet lines indicate the evolutions for $s = 1, 3, 5$, and 7, respectively.

results for $\alpha = 2$ in Fig. 4 are consistent with Chasnov's[31] results. Furthermore, the present numerical simulations imply that the critical initial Reynolds numbers for $\alpha = 1$ and 3 are $Re_c > 100$ and $Re_c < 100$, respectively. In particular, since the Reynolds number for $\alpha = 1$ evolves slightly, we expect that the critical initial Reynolds number for $\alpha = 1$ is very close to 100. We will show that the enstrophy spectra evolve in an approximately self-similar manner for $\alpha = 1$ in Sec. V B. There is little difference between the evolution of Re for $s = 3, 5$, and 7.

The temporal evolution of the integral scale defined by the correlation function of the vorticity field q,[28]

$$\ell_q \equiv \frac{1}{\langle q^2 \rangle} \int_0^\infty \langle q q' \rangle \, \mathrm{d}r = \frac{2}{\langle q^2 \rangle} \int_0^\infty \frac{Q_\alpha(k)}{k} \, \mathrm{d}k, \tag{44}$$

is shown in Fig. 5. Note that since ℓ_q depends only on the form of the enstrophy spectrum, ℓ_q is initially independent of the value of α. For $\alpha = 1, 2$, the algebraic exponent of the evolution of ℓ_q

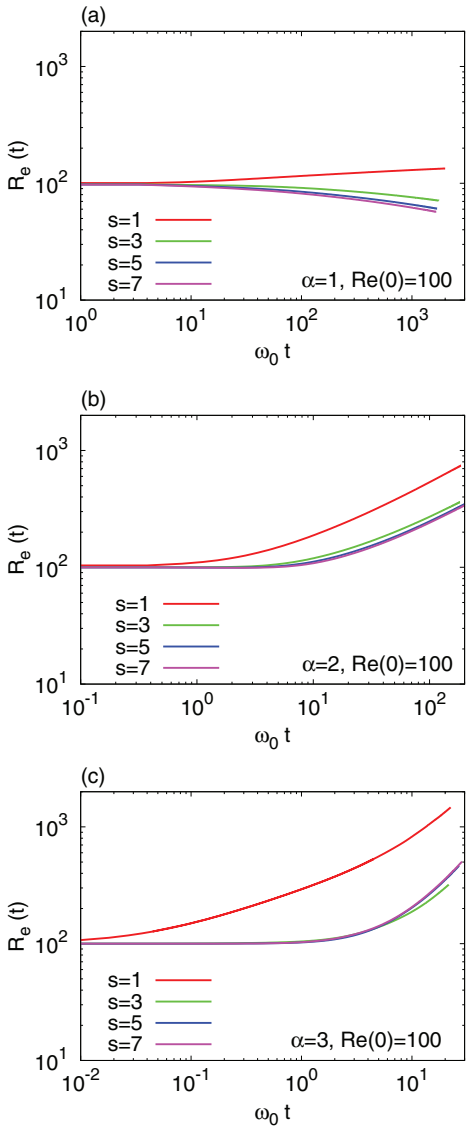

FIG. 4. Time evolution of Reynolds number, $Re(t)$, for (a) $\alpha = 1$, (b) $\alpha = 2$, and (c) $\alpha = 3$. The red, green, blue, and violet lines indicate the evolutions for $s = 1, 3, 5$, and 7, respectively.

is approximately independent of s. For $\alpha = 2$, the growth of the integral scale is well represented by $\ell_q \sim t^{0.5}$. This is consistent with previous studies.[28,38,39] For $\alpha = 1$, the growth of the integral scale behaves as $\ell_q \sim t^{0.4}$. In contrast, for $\alpha = 3$, ℓ_q increases monotonically with time for $s = 1$ but decreases slightly at $\omega_0 t = 1 \sim 4$ and then increases asymptotically for $s = 3, 5$, and 7. For $\alpha = 3$ with $s = 3, 5$, and 7, the integral scale behaves as $\ell_q \sim t^{0.5}$, although the scaling range is somewhat short compared to the cases of $\alpha = 1$ and 2. The above results indicate that the algebraic evolution of the integral scale of the vorticity field from narrow initial spectra is approximately independent of the value of α.

Next, we consider the main topic of the present paper. In order to examine the results of Sec. III, the enstrophy spectra at logarithmically equal time intervals are shown in Figs. 6, 7, and 8 for $\alpha = 1, 2$, and 3, respectively. For the evolution from the initial condition with $s = 1$, the initial slope of the enstrophy spectrum is preserved near the lowest wavenumbers. This indicates the conservation of J, which is defined by Eq. (6b). As time goes by, $Q_\alpha(k) \sim Jk$ spectra are progressively

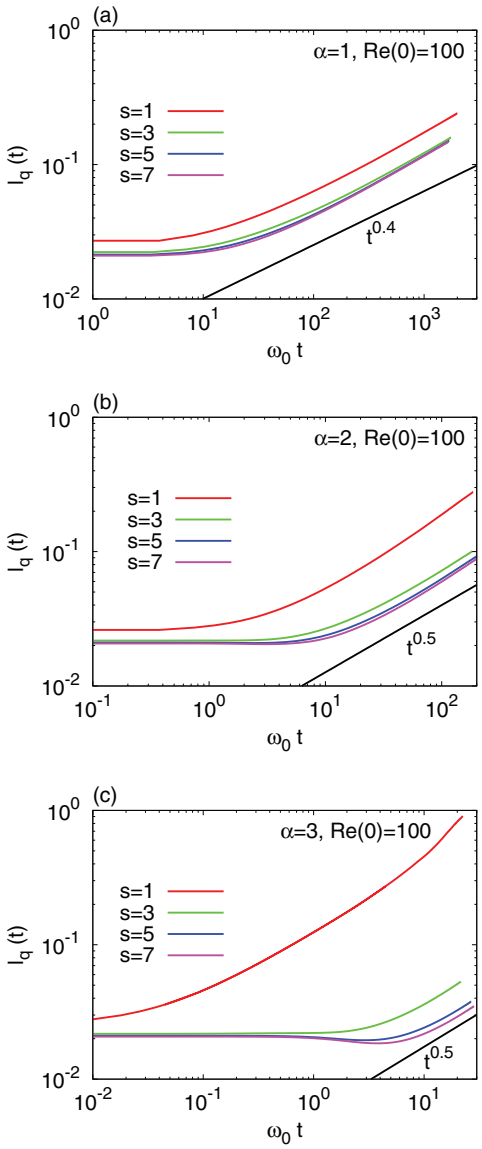

FIG. 5. Time evolution of the integral scale of the vorticity field, $\ell_q(t)$, for (a) $\alpha = 1$, (b) $\alpha = 2$, and (c) $\alpha = 3$. The red, green, blue, and violet lines indicate the evolutions for $s = 1, 3, 5$, and 7, respectively.

overshadowed by a steeper spectrum from the higher-wavenumber side for $\alpha = 1$ and 2. For $\alpha = 3$, the Jk spectrum decays while maintaining their initial form in the low-wavenumber range. For $s = 3$, the enstrophy spectrum near the lowest-wavenumber range evolves only slightly, and the $Q_\alpha(k) \sim Lk^3$ spectrum is invaded by a steeper spectrum from the higher-wavenumber side, in the same manner as for $s = 1$. This indicates that L, which is defined by Eq. (6c), is conserved during the evolution. The steeper spectrum overshadowing from the higher-wavenumber side is somewhat shallower than the theoretically expected k^5 spectrum. Based on the evolution from the initial spectrum with $s = 5$, it is clear that the low-wavenumber spectrum is the form of $Q_\alpha(k) \sim k^5$ for all α. For $s = 7$, the initial spectra quickly adjust to the k^5 spectra, and then the k^5 spectra preserve their forms. These results are in line with the theoretical predictions obtained in Sec. III.

Finally, we compare the theoretical predictions in Sec. III with the results of the numerical simulations in detail. In Sec. III, we assumed that the viscous term in the evolution equation for the

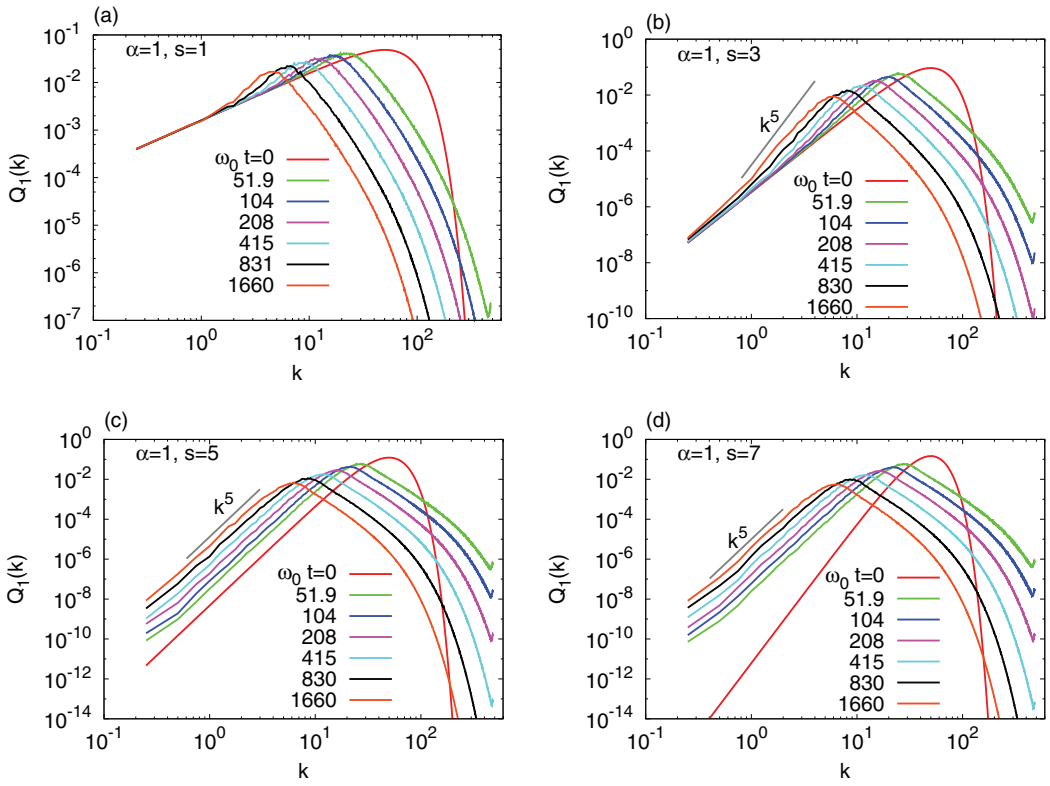

FIG. 6. Evolution of the enstrophy spectrum for $\alpha = 1$ starting with (a) $s = 1$, (b) $s = 3$, (c) $s = 5$, and (d) $s = 7$. The plotted times correspond to $\omega_0 t = 0, 51.9, 104, 208, 415, 830$, and 1660.

enstrophy spectrum, Eq. (13), is negligible in the infrared range. Then, the enstrophy spectrum can be formally written as

$$Q_\alpha(k,t) = Q_\alpha(k,0) + \int_0^t T_\alpha^{\mathcal{Q}}(k,s)\,\mathrm{d}s. \tag{45}$$

In order to validate the above assumption, we compare the enstrophy spectrum calculated by Eq. (12b) and that evaluated by the right-hand side of Eq. (45). Figure 9 shows the case for $\alpha = 1$ starting with $s = 5$ as an example. The agreement between both spectra is good in the low-wavenumber range. Since the first term on the right-hand side of Eq. (45) is greater than the second term in the early stage of evolution, the influence of the initial condition remains in the form of the enstrophy spectrum. This is the reason why the spectra $Q_\alpha(k) \sim k^1$ and k^3 are observed transiently for $s = 1$ and 3, respectively. On the other hand, when sufficient time passes, the enstrophy spectrum at that time is dominated by the second term on the right-hand side of Eq. (45). Therefore, the power law of the enstrophy spectrum at later times is generated by the second term on the right-hand side of Eq. (45). Thus, we express the wavenumber dependence of the enstrophy transfer function in the low wavenumber range as follows:

$$\int_0^t T_\alpha^{\mathcal{Q}}(k,s)\mathrm{d}s = C(t)k^{b(t)}, \tag{46}$$

and examine the dependence of the exponent b on α and s. Figure 10 shows the evolution of $b(t)$. Here, we calculate the integral using Simpson's trapezoidal formula and evaluate the exponent b over the ranges $0.75 \le k \le 2.5$. Note that the theoretical prediction in Sec. III was $T_\alpha^{\mathcal{Q}}(k \to 0) \sim k^5$, independent of the initial condition. When the enstrophy transfer function is negative, the value

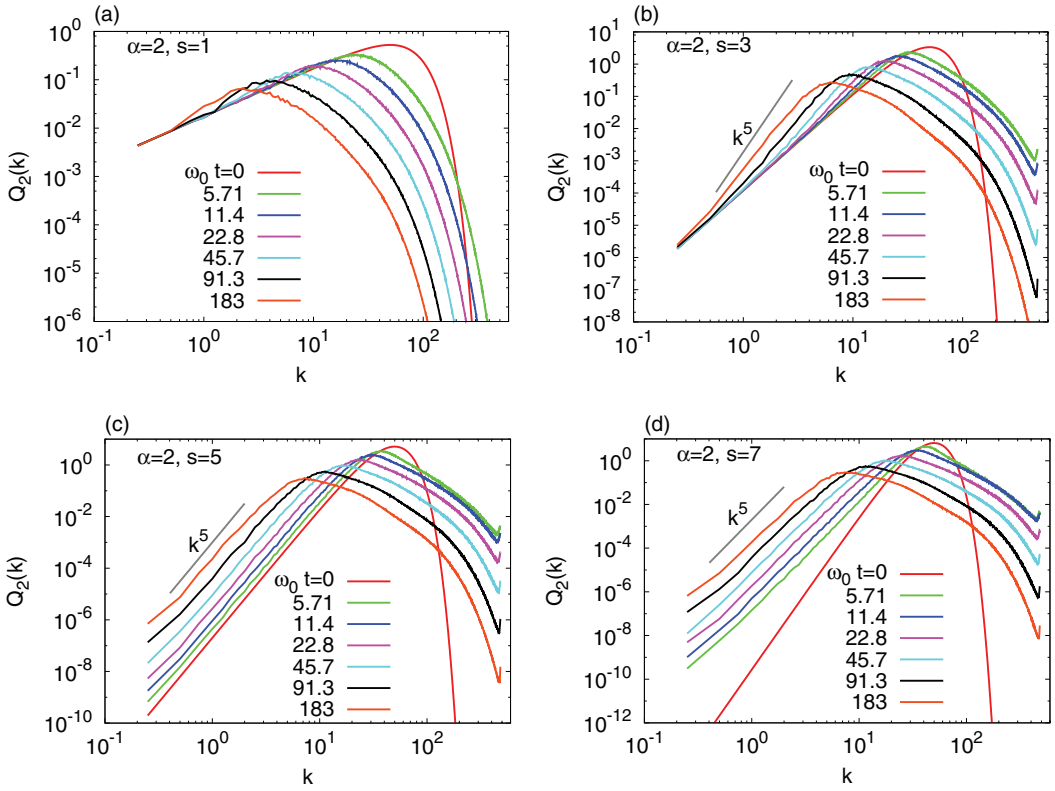

FIG. 7. Evolution of the enstrophy spectrum for $\alpha = 2$ with (a) $s = 1$, (b) $s = 3$, (c) $s = 5$, and (d) $s = 7$. The plotted times correspond to $\omega_0 t = 0, 5.71, 11.4, 22.8, 45.7, 91.3$, and 183.

of $b(t)$ is not shown at that time in the figure. For three cases, $\alpha = 1$ with $s = 1$, $\alpha = 3$ with $s = 1$, and $\alpha = 3$ with $s = 3$, the enstrophy transfer function is negative in the ranges $0.75 \le k \le 2.5$ over the simulation period. In addition, for $\alpha = 2$ with $s = 1$, the transfer function fluctuates between positive and negative values, and b deviates significantly from the theoretically predicted value. Thus, we cannot obtain the theoretical results $T_\alpha^{\mathcal{Q}}(k \to 0) \sim k^5$ for these cases. For other cases, $b(t)$ asymptotically approaches the theoretically predicted value after an initial transient, but gradually decreases. The deviation of b from the theoretical value would be responsible for the finiteness of the flow domain. One effect of the finiteness of the flow domain is the accumulation of energy and enstrophy by the backscatter. On the other hand, progressing the spectral peak to the lower wavenumber side narrows the low-wavenumber range due to the finiteness of the flow domain. In this case, the assumption of neglecting the eddy viscosity term in Eq. (32a) would be violated. When $Q_\alpha(k) \sim k^\gamma$ with $\gamma > 1$, the eddy viscosity coefficient $\nu_{\mathrm{T}}^{(+)}$ is a positive quantity, and the eddy viscosity term contributes to shallowing of the enstrophy spectrum in the low-wavenumber range. This is another effect of the finiteness of the flow domain.

V. DISCUSSION

A. Comparison with previous results

First, we show that the theoretical results in Sec. III are consistent with previous studies on the infrared spectra of NS($\alpha = 2$) and CHM($\alpha = -2$) turbulence. Next, we compare the results of the present study with the SQG($\alpha = 1$) case studied by Tran and Dritschel.[33] We further comment on an interpretation of their work and an application of their calculations to the system with arbitrary α.

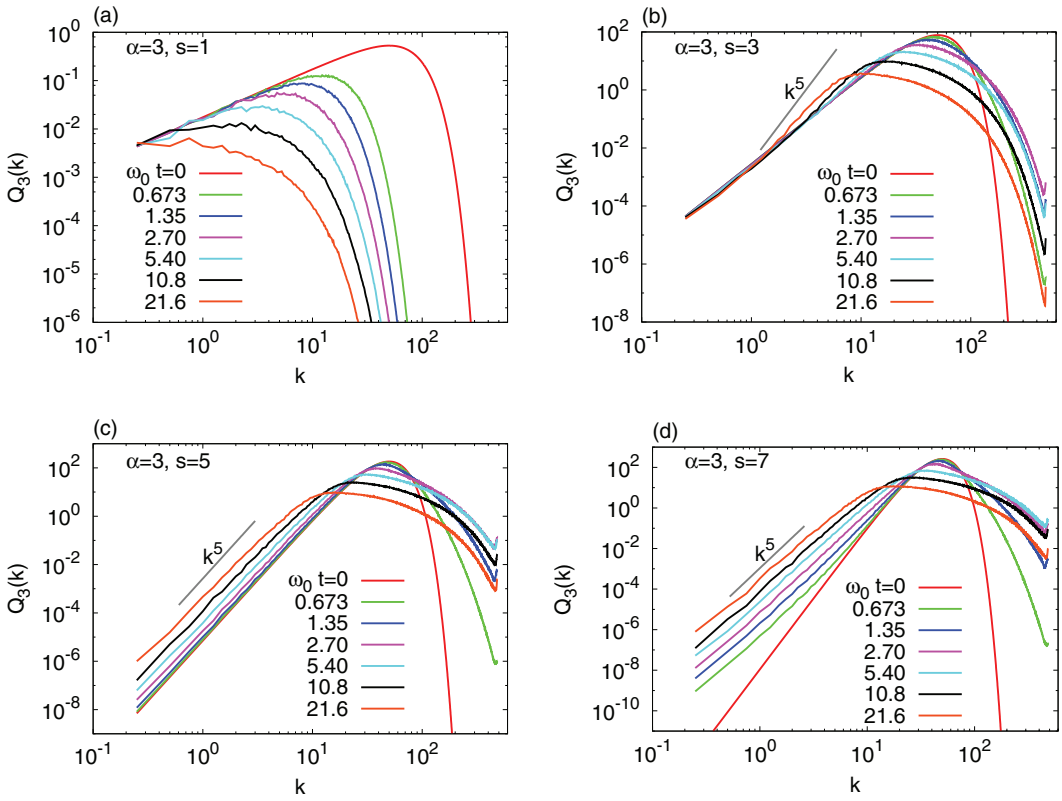

FIG. 8. Evolution of the enstrophy spectrum for $\alpha = 3$ starting with (a) $s = 1$, (b) $s = 3$, (c) $s = 5$, and (d) $s = 7$. The plotted times correspond to $\omega_0 t = 0, 0.673, 1.35, 2.70, 5.40, 10.8$, and 21.6.

1. $\alpha = 2$ case

For $\alpha = 2$, the relationship between the energy spectrum and the enstrophy spectrum is given as follows:

$$Q_2(k) = k^2 E_2(k). \tag{47}$$

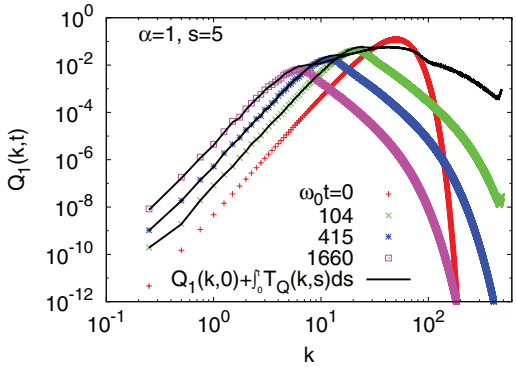

FIG. 9. Enstrophy spectra for $\alpha = 1$ with $s = 5$ at $\omega_0 t = 0$, 104, 415, and 1660. The black lines indicate the evaluated enstrophy spectrum according to Eq. (45) at corresponding times. The integral in Eq. (45) was evaluated by Simpson's trapezoidal method.

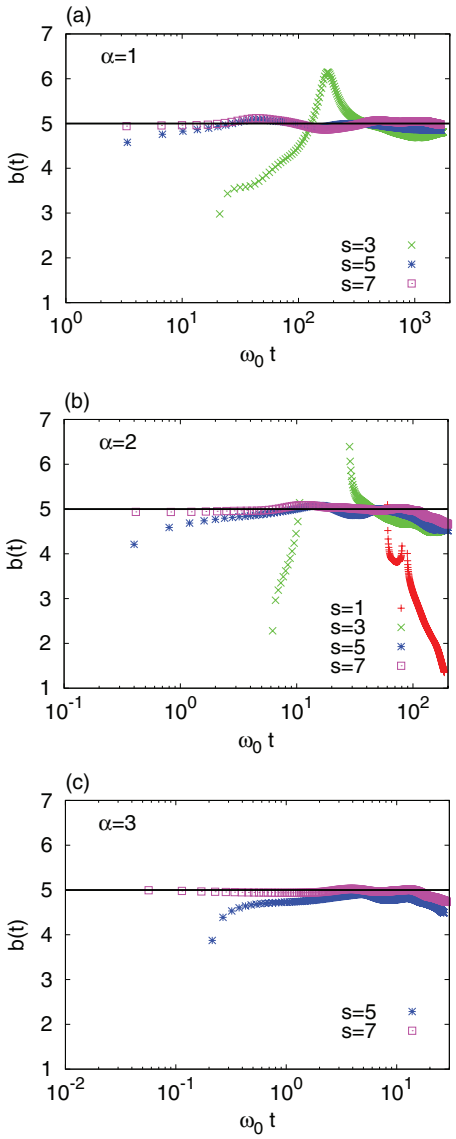

FIG. 10. Time evolution of the exponent $b(t)$ defined by Eq. (46) for (a) $\alpha = 1$, (b) $\alpha = 2$, and (c) $\alpha = 3$. Red, green, blue, and purple indicate data for $s = 1, 3, 5$, and 7, respectively. Negative enstrophy transfer is not plotted.

Thus, the infrared enstrophy spectrum of the form $Q_2(k) \propto k^5$ is equivalent to the infrared energy spectrum of the form $E_2(k) \propto k^3$, which is consistent with the previous study on the infrared energy spectrum of NS turbulence.[24,27,32] Moreover, using Eq. (47), Eqs. (32a) and (32b) are reduced as follows:

$$T_2^{\mathcal{Q}(-)}{}_{\mathrm{NL}}(k) \simeq \left[\int_{k/\epsilon}^{\infty} \theta_{kll}\, l^{-1}\{E_2(l)\}^2\, \mathrm{d}l\right] k^5 - 2\nu_{\mathrm{T}}^{(+)}(k) k^4 E_2(k) \tag{48a}$$

and

$$\nu_{\mathrm{T}}^{(+)}(k) \equiv \frac{1}{4}\int_{k/\epsilon}^{\infty} \theta_{kll}\, \frac{\partial\{l E_2(l)\}}{\partial l}\, \mathrm{d}l, \tag{48b}$$

respectively, for $\alpha = 2$. Eq. (48) is consistent with the kth derivative of Eq. (2.7) with Eq. (2.8) of BLS78. Note that since BLS78 defined the kinetic energy by $\overline{\boldsymbol{v}^2}$, we should multiply the factor 2 by Eq. (2.7) of BLS78 when we compare Eq. (2.7) of BLS78 with Eq. (48).

2. $\alpha = -2$ case

The CHM equation in the strong turbulent state neglecting the effects of waves, dissipation, and forcing can be written as follows:

$$\frac{\partial}{\partial t}\left(\nabla^2\psi - \lambda^2\psi\right) + J(\psi,\ \nabla^2\psi) = 0, \tag{49}$$

where the constant λ is either the ratio of the horizontal length scale of interest L to the ion Larmor radius in the plasma case or the ratio of L to the Rossby deformation radius in the geophysical case. Equation (49) has two quadratic inviscid invariants: the total energy, $\mathcal{E}_{\text{total}} = \left\{\overline{(\nabla\psi)^2} + \overline{\lambda^2\psi^2}\right\}/2$, and the potential enstrophy, $\mathcal{Z} = \left\{\overline{(\nabla^2\psi)^2} + \lambda^2\overline{(\nabla\psi)^2}\right\}/2$. In the AM regime ($\lambda \to \infty$), the governing equation given by Eq. (49) is reduced as follows:

$$\frac{\partial\psi}{\partial T} + J(\nabla^2\psi, \psi) = 0, \tag{50}$$

where $T = t/\lambda^2$ is a rescaled time. Furthermore, the total energy and potential enstrophy are reduced to $\mathcal{E}_{\text{total}} \to \lambda^2\overline{\psi^2}/2$ and $\mathcal{Z} \to \lambda^2\overline{(\nabla\psi)^2}/2$, respectively. Comparing Eqs. (1) and (50) indicates that the stream function ψ and the ordinary vorticity $\nabla^2\psi$ in the CHM-AM system play the roles of the generalized vorticity and the stream function, respectively, in the generalized 2D fluid system. Therefore, the invariants $\mathcal{E}_{\text{total}}$ and $\mathcal{Z}$ correspond to the generalized enstrophy $\mathcal{Q}_{-2}$ and the generalized energy $\mathcal{E}_{-2}$, respectively. More precisely, $\mathcal{E}_{\text{total}} = \lambda^2\mathcal{Q}_{-2}$ and $\mathcal{Z} = \lambda^2\mathcal{E}_{-2}$ in the AM regime. Hence, the generalized enstrophy spectrum in the infrared range for $\alpha = -2$, $Q_{-2}(k) \propto k^5$, derived in the present study is consistent with the total energy spectrum in the infrared range for the CHM-AM turbulence, $E_{\text{total}}(k) \propto k^5$, derived by Iwayama *et al.*[26] Moreover, the generalized enstrophy transfer function, Eq. (32a), for $\alpha = -2$ is written as

$$T^{\mathcal{Q}\,(-)}_{-2\text{NL}}(k) \simeq \left[\int_{k/\epsilon}^{\infty} \theta_{kll}\, l^3 \{Q_{-2}(l)\}^2\, \mathrm{d}l\right] k^5 - 2\nu_{\text{T}}^{(-)}(k) k^4 Q_{-2}(k), \tag{51a}$$

with

$$\nu_{\text{T}}^{(-)}(k) \equiv \frac{1}{4}\int_{k/\epsilon}^{\infty} \theta_{kll}\, l^4 \frac{\partial\,\{l\,Q_{-2}(l)\}}{\partial l}\,\mathrm{d}l. \tag{51b}$$

These are also consistent with Eqs. (3.9) and (3.10) in Iwayama *et al.*[26]

3. $\alpha = 1$ case

As mentioned in Sec. I, Tran and Dritschel[33] derived that the kinetic energy spectrum has k^5 dependence at small wavenumbers for the SQG system. We note that this is consistent with the k^5 generalized enstrophy spectrum in the infrared range derived in the present study, because the kinetic energy is the generalized enstrophy for the SQG system:

$$\mathcal{K} = \frac{1}{2}\overline{(\nabla\psi)^2} = \frac{1}{2}\overline{\{(-\nabla^2)^{1/2}\psi\}^2} = \mathcal{Q}_1. \tag{52}$$

We interpret the work by Tran and Dritschel[33] and consider an application of their calculations to the other values of α. They first focused their attention on the stream function, because it is a quantity characterizing the large-scale dynamics. We should note that they had not used a condition that the wavenumber of interest k belongs to the infrared range or k is a small number.

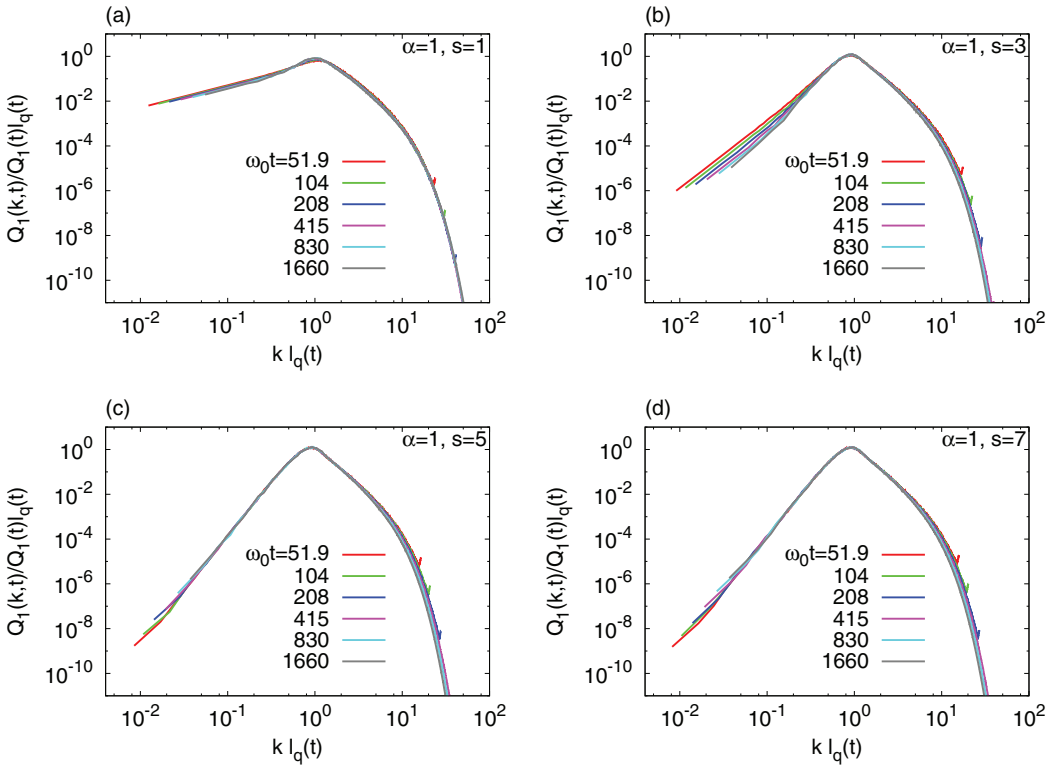

FIG. 11. Normalized enstrophy spectra for $\alpha = 1$ with (a) $s = 1$, (b) $s = 3$, (c) $s = 5$, and (d) $s = 7$. The abscissa is normalized by ℓ_q, and the ordinate is normalized by $\mathcal{Q}_1(t)\ell_q(t)$. The plotted times correspond to $\omega_0 t = 51.9, 104, 208, 415, 830$, and 1660.

Then, they expressed the upper bound for the time derivative of $|\hat{\psi}(\boldsymbol{k})|$ in terms of the generalized energy, $\mathcal{E}_\alpha$, which is an upward cascading quantity and an invariant, by using the Cauchy-Schwarz inequality and a triad relationship between wavenumbers. The previous and present works on the infrared spectrum show that the infrared spectrum is formed by the interactions between the infrared wavenumbers and the energy-enstrophy centroid wavenumbers.[24,26] In this sense, their idea is physically reasonable. Thus, we expect the application of their calculations to the system with arbitrary α. Indeed, we can express $\mathrm{d}|\hat{\psi}(\boldsymbol{k})|/\mathrm{d}t$ in terms of $\mathcal{E}_\alpha$ using a dimensional analysis as follows:

$$\frac{\mathrm{d}}{\mathrm{d}t}|\hat{\psi}(\boldsymbol{k})| \sim k^{2-\alpha}\mathcal{E}_\alpha. \tag{53}$$

Because the right-hand side of (53) is expressed in term of time-independent quantities, we formally integrate (53) and then obtain the evolution of the modal stream function,

$$|\hat{\psi}(\boldsymbol{k})| \sim k^{2-\alpha}\mathcal{E}_\alpha t. \tag{54}$$

Using (54), the generalized enstrophy spectrum $Q_\alpha(k)$ is expressed as

$$Q_\alpha(k) \sim \frac{1}{2}k\left(k^\alpha|\hat{\psi}(\boldsymbol{k})|\right)^2 \sim k^5\mathcal{E}_\alpha t^2. \tag{55}$$

The k^5 dependence of the generalized enstrophy spectrum on the wavenumbers is consistent with the infrared spectrum that we have discussed in the present study. However, for $\alpha < 0$, a quantity characterizing large-scale flows is not the stream function ψ but the generalized vorticity q, and the upward cascading quantity is not the generalized energy $\mathcal{E}_\alpha$ but the generalized enstrophy $\mathcal{Q}_\alpha$.

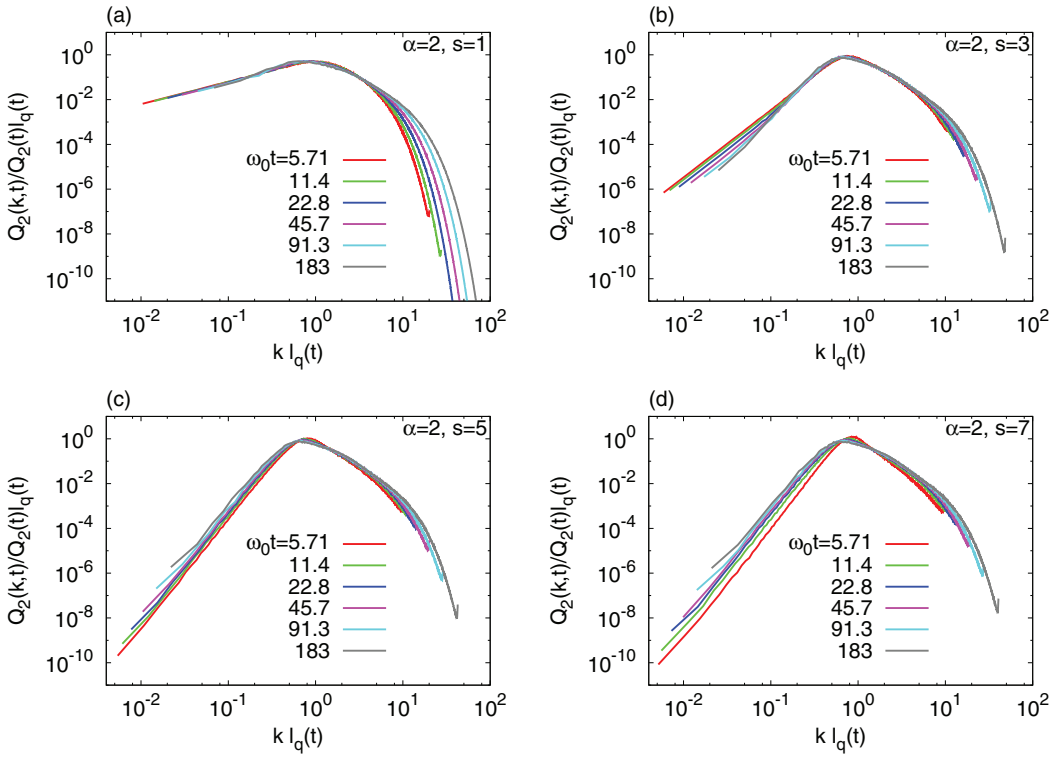

FIG. 12. Normalized enstrophy spectra for $\alpha = 2$ with (a) $s = 1$, (b) $s = 3$, (c) $s = 5$, and (d) $s = 7$. The abscissa is normalized by ℓ_q, and the ordinate is normalized by $\mathcal{Q}_2(t)\ell_q(t)$. The plotted times correspond to $\omega_0 t = 5.71, 11.4, 22.8, 45.7, 91.3$, and 183.

Therefore, it is impossible to interpret that their calculations represent the large-scale dynamics for $\alpha < 0$. Furthermore, we cannot express the upper bound for the evolution of the modal stream function in terms of $k^{2-\alpha}\mathcal{E}_\alpha$ except for $\alpha = 1$ and 2 by using only the Cauchy-Schwarz inequality and the triad relation. (See Appendix C for details.) For these reasons, the calculations by Tran and Dritschel[33] work only for $\alpha = 1$ and 2.

B. Self-similarity of enstrophy spectrum

We examine the self-similarity of the enstrophy spectrum obtained in Sec. IV. The self-similarity depends on the initial Reynolds number. For example, Chasnov[31] demonstrated that the energy spectrum for decaying NS turbulence at the critical initial Reynolds number $Re_c = 15.73$ exhibits the self-similar evolution. On the other hand, the energy spectrum at a moderate initial Reynolds number is not self-similar.[28,31,32] As mentioned in Sec. IV, we can expect the self-similarity evolution of the enstrophy spectrum for $\alpha = 1$ with $s = 5$ and 7, because the Reynolds number remains approximately constant after the initial transient. Figures 11–13 show the normalized enstrophy spectra. Here the wavenumber k is normalized by ℓ_q, and $Q_\alpha(k)$ by $\mathcal{Q}_\alpha \ell_q$. Figure 11 shows that the enstrophy spectrum for $\alpha = 1$ with $s = 5$ and 7 are almost self-similar over the entire wavenumber range. This result indicates that the critical initial Reynolds number for $\alpha = 1$ is approximately $Re_c = 100$. The enstrophy spectrum for $\alpha = 1$ with $s = 1$ appears to be self-similar as well. However, since the low-wavenumber range spectrum is progressively overshadowed by the steeper spectrum from higher wavenumbers, exact self-similarity is not expected. There is some evidence of this in the form of a bump growing around $k\ell_q = 1$. For $\alpha = 2$ and $\alpha = 3$, as shown in Figs. 12 and 13, the enstrophy spectra are not self-similar, as inferred from the evolution of the Reynolds number.

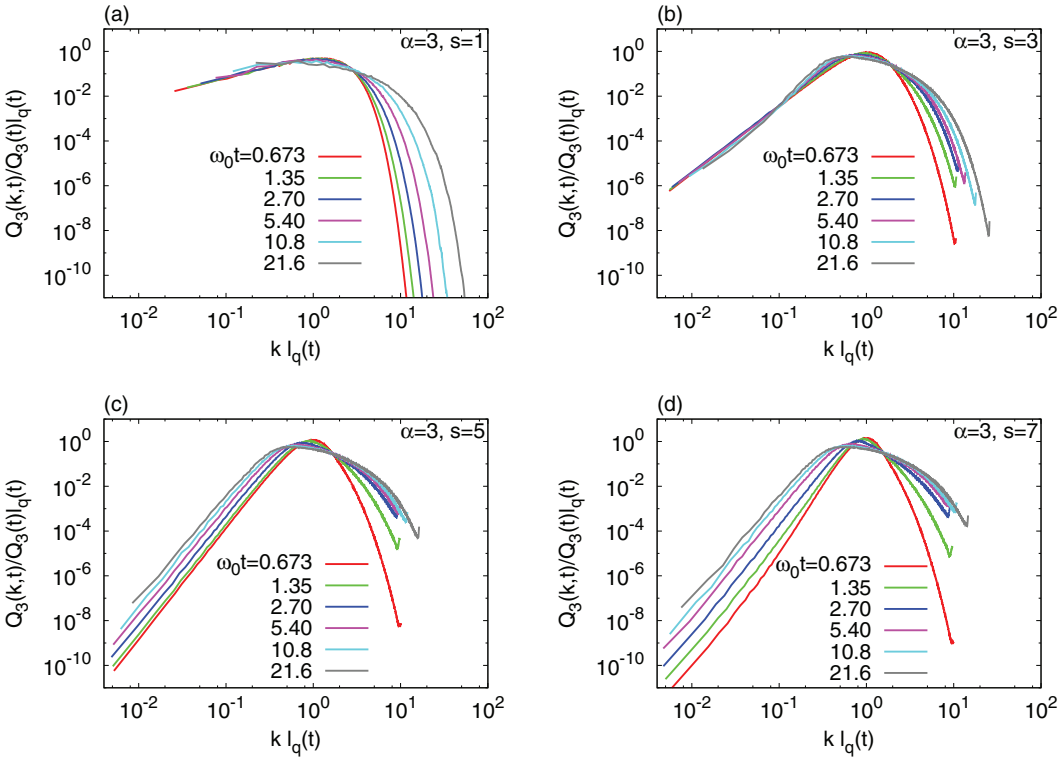

FIG. 13. Normalized enstrophy spectra for $\alpha = 3$ with (a) $s = 1$, (b) $s = 3$, (c) $s = 5$, and (d) $s = 7$. The abscissa is normalized by ℓ_q, and the ordinate is normalized by $\mathcal{Q}_3(t)\ell_q(t)$. The plotted times correspond to $\omega_0 t = 0.673, 1.35, 2.70, 5.40, 10.8$, and 21.6.

VI. SUMMARY

We have examined the low-wavenumber behavior of decaying turbulence governed by the generalized 2D fluid system theoretically and by direct numerical simulation. The enstrophy transfer function in the infrared range ($k \to 0$) was theoretically derived to be $T_\alpha^{\mathcal{Q}}(k \to 0) \sim k^5$ using a quasi-normal Markovianized model of the generalized 2D fluid system. This led to three canonical cases of infrared enstrophy spectra, which depend on the initial conditions: $Q_\alpha(k \to 0) \sim Jk$, $Q_\alpha(k \to 0) \sim Lk^3$, and $Q_\alpha(k \to 0) \sim Ik^5$. The prefactors J and L were demonstrated to be invariants of the system, but I was an increasing function of time. The evolution from a narrow initial enstrophy spectrum exhibits the universal infrared enstrophy spectrum of the form $Q_\alpha(k \to 0) \sim k^5$, which is independent of α. Both spectra, $Q_\alpha(k) \sim Jk$ and $Q_\alpha(k) \sim Lk^3$, are observed transiently and eventually overshadowed by the k^5 spectrum. These results have been verified by direct numerical simulations of decaying α-turbulence.

The $Q_\alpha(k) \sim Jk$ scaling is singular in the sense that the corresponding energy spectrum, $E_\alpha(k) \sim Jk^{1-\alpha}$, takes the infrared divergence for $\alpha > 1$. Similarly, the $Q_\alpha(k) \sim Lk^3$ and Ik^5 scalings are singular for $\alpha > 3$ and $\alpha > 5$, respectively. However, as reported by Iwayama and Watanabe,[9] the physical relevant system of the generalized 2D fluid system must be $\alpha \leq 3$. Thus, only the $Q_\alpha(k) \sim Jk$ scaling for $1 < \alpha \leq 3$ is singular for the physical relevant system.

Based on the direct numerical simulation of the decaying α-turbulence, we showed that the enstrophy spectrum evolves in a self-similar manner over the entire wavenumber range at the initial Reynolds number $Re \approx 100$ for $\alpha = 1$. In the future, the critical initial Reynolds number should be determined precisely for any value of α.

ACKNOWLEDGMENTS

The present study was supported by a Grant-in-Aid for Scientific Research (C) No. 24540472 from the Japanese Society for the Promotion of Science. We would like to thank two anonymous reviewers for their constructive suggestions. T.I. would like to thank all of the members of the Atmospheric Science Group of Kobe University and Professor T. Yajima of Utsunomiya University for helpful conversations on this topic.

APPENDIX A: DERIVATION OF EQ. (31)

Substituting Eq. (23) into Eq. (22) and using the sine law,

$$\frac{\sqrt{1-x^2}}{k} = \frac{\sqrt{1-z^2}}{m}, \tag{A1}$$

the triad enstrophy transfer function Eq. (22) is written as

$$T_\alpha^{\mathcal{Q}}(k',l,m) = \frac{4k'\sqrt{1-z^2}}{\pi l^{\alpha-1}m^\alpha}\theta_{k'lm}\left[\frac{(m^\alpha-l^\alpha)^2}{(lm)^\alpha}k'Q_\alpha(l)Q_\alpha(m)\right.$$
$$\left. - \frac{(m^\alpha-l^\alpha)}{k'^\alpha}\left\{\frac{l(m^\alpha-k'^\alpha)}{m^\alpha}Q_\alpha(m) - \frac{m(l^\alpha-k'^\alpha)}{l^\alpha}Q_\alpha(l)\right\}Q_\alpha(k')\right]. \tag{A2}$$

In order to expand Eq. (A2) in $\epsilon = k'/l$, we perform some preliminary calculations. From the cosine law Eq. (28), the following formulae are obtained

$$m^\alpha = l^\alpha\left[1-\alpha z\epsilon + \mathcal{O}(\epsilon^2)\right], \tag{A3}$$

$$m^\alpha - l^\alpha = l^\alpha\left[-\alpha z\epsilon + \mathcal{O}(\epsilon^2)\right], \tag{A4}$$

$$(m^\alpha - l^\alpha)^2 = l^{2\alpha}\left[\alpha^2z^2\epsilon^2 + \mathcal{O}(\epsilon^3)\right], \tag{A5}$$

$$m^\alpha - k'^\alpha = m^\alpha - l^\alpha\epsilon^\alpha = l^\alpha\left[1-\epsilon^\alpha-\alpha z\epsilon + \mathcal{O}(\epsilon^2)\right], \tag{A6}$$

$$l^\alpha - k'^\alpha = l^\alpha(1-\epsilon^\alpha). \tag{A7}$$

Moreover, the enstrophy spectrum can be expanded as

$$Q_\alpha(m) = Q_\alpha\left(l\left\{1-\epsilon z + \mathcal{O}(\epsilon^2)\right\}\right)$$
$$= Q_\alpha(l) - lz\epsilon\frac{\partial Q_\alpha(l)}{\partial l} + \mathcal{O}(\epsilon^2). \tag{A8}$$

Using the above equations, the leading order term of the first term in the angle brackets of Eq. (A2) yields

$$\frac{(m^\alpha-l^\alpha)^2}{(lm)^\alpha}k'Q_\alpha(l)Q_\alpha(m) \simeq \alpha^2z^2k'\epsilon^2\left\{Q_\alpha(l)\right\}^2. \tag{A9}$$

The leading order terms of the second term in the angle brackets of Eq. (A2) are

$$\begin{aligned}
&\frac{m^\alpha - l^\alpha}{k'^\alpha}\left[\frac{l(m^\alpha - k'^\alpha)}{m^\alpha}Q_\alpha(m) - \frac{m(l^\alpha - k'^\alpha)}{l^\alpha}Q_\alpha(l)\right]Q_\alpha(k') \\
&\quad = -\frac{\alpha l^{\alpha+1}z\epsilon}{k'^\alpha}\left[\left(1+\alpha z\epsilon+\mathcal{O}(\epsilon^2)\right)\left(1-\epsilon^\alpha-\alpha z\epsilon+\mathcal{O}(\epsilon^2)\right)\left(Q_\alpha(l) - lz\epsilon\frac{\partial Q_\alpha(l)}{\partial l}+\mathcal{O}(\epsilon^2)\right)\right. \\
&\quad \left. -\left(1-z\epsilon+\mathcal{O}(\epsilon^2)\right)(1-\epsilon^\alpha)Q_\alpha(l)\right]Q_\alpha(k') \\
&\quad \simeq -\frac{\alpha l^{\alpha+1}z^2\epsilon^2}{k'^\alpha}\left[\left\{2Q_\alpha(l) - \frac{\partial\{lQ_\alpha(l)\}}{\partial l}\right\} - \left\{(\alpha+2)Q_\alpha(l) - \frac{\partial\{lQ_\alpha(l)\}}{\partial l}\right\}\epsilon^\alpha\right]Q_\alpha(k').
\end{aligned} \tag{A10}$$

When $\alpha > 0$, the first term in the angle brackets of Eq. (A10) is its leading order term, whereas the second term is its leading order term when $\alpha < 0$. Moreover, the leading order of $\theta_{k'lm}$ is

$$\begin{aligned}
\theta_{k'lm} &= \mu^{-1}\left\{l^{5-2\alpha}Q_\alpha(l)\right\}^{-1/2}\left[1+\left(\frac{k'^{5-2\alpha}Q_\alpha(k')}{l^{5-2\alpha}Q_\alpha(l)}\right)^{1/2}+\left(\frac{m^{5-2\alpha}Q_\alpha(m)}{l^{5-2\alpha}Q_\alpha(l)}\right)^{1/2}\right]^{-1} \\
&\simeq \theta_{k'll}.
\end{aligned} \tag{A11}$$

Here, $\theta_{k'll}$ is independent of k' provided that $Q_\alpha(k) \sim k^n$ with $n \geq 2\alpha - 5$. Note that there are no contradictions between this assumption and the resulting infrared spectrum.

Substituting Eqs. (A9) and (A11) into Eq. (A2) yields

$$\begin{aligned}
T_\alpha^{\mathcal{Q}}(k', l, z) &\simeq \frac{4k'z^2\sqrt{1-z^2}}{\pi l^{2\alpha-1}}\theta_{k'll}\,\epsilon^2\left[\alpha^2 k'\{Q_\alpha(l)\}^2\right. \\
&\qquad -\frac{\alpha l^{\alpha+1}}{k'^\alpha}\left\{\frac{\partial\{lQ_\alpha(l)\}}{\partial l} - 2Q_\alpha(l)\right\}Q_\alpha(k')H(\alpha) \\
&\qquad \left. +\frac{\alpha l^{\alpha+1}}{k'^\alpha}\epsilon^\alpha\left\{\frac{\partial\{lQ_\alpha(l)\}}{\partial l} - (\alpha+2)Q_\alpha(l)\right\}Q_\alpha(k')H(-\alpha)\right] \\
&= \frac{4z^2\sqrt{1-z^2}}{\pi}\theta_{k'll}\left[\alpha^2 l^{-(2\alpha+1)}\{Q_\alpha(l)\}^2 k'^4\right. \\
&\qquad -\alpha l^{-\alpha}\left\{\frac{\partial\{lQ_\alpha(l)\}}{\partial l} - 2Q_\alpha(l)\right\}k'^{3-\alpha}Q_\alpha(k')H(\alpha) \\
&\qquad \left. +\alpha l^{-2\alpha}\left\{\frac{\partial\{lQ_\alpha(l)\}}{\partial l} - (\alpha+2)Q_\alpha(l)\right\}k'^3 Q_\alpha(k')H(-\alpha)\right].
\end{aligned} \tag{A12}$$

Here, $H(x)$ is the Heaviside step function, which is defined by

$$H(x) = \begin{cases} 0, & (x < 0), \\ 1, & (x > 0). \end{cases} \tag{A13}$$

APPENDIX B: BESSEL FUNCTION FORMULAE

The Bessel function of the first kind of order zero is defined as follows:

$$J_0(x) = \frac{1}{\pi}\int_0^\pi \cos(x\cos\theta)\,\mathrm{d}\theta, (x \geq 0). \tag{B1}$$

Using the series expression, $J_0(x)$ is expressed as

$$J_0(x) = \sum_{k=0}^{\infty} \left(-\frac{1}{4}\right)^k \frac{1}{(k!)\Gamma(k+1)} x^{2k} \tag{B2}$$

$$= 1 - \frac{1}{4}x^2 + \frac{1}{64}x^4 - \frac{1}{2304}x^6 + \mathcal{O}(x^8). \tag{B3}$$

The integral of $J_0(x)$ is

$$\int_0^{\infty} J_0(ax)\,\mathrm{d}x = \frac{1}{a}, (a > 0). \tag{B4}$$

APPENDIX C: APPLICATIONS OF CALCULATIONS BY TRAN AND DRITSCHEL (2006) TO THE SYSTEM WITH $0 < \alpha \leq 3$

The starting point of their calculations is the evolution equation for the modal stream function $\hat{\psi}(\boldsymbol{k})$,

$$\frac{\mathrm{d}}{\mathrm{d}t}\hat{\psi}(\boldsymbol{k}) = \sum_{\boldsymbol{l}}\sum_{\boldsymbol{m}} \delta_{\boldsymbol{k},\boldsymbol{l}+\boldsymbol{m}} \frac{l^\alpha - m^\alpha}{2k^\alpha} (\boldsymbol{m}\times\boldsymbol{l})_z \hat{\psi}(\boldsymbol{l})\hat{\psi}(\boldsymbol{m}). \tag{C1}$$

We note in passing that the factor 1/2 is dropped in the nonlinear term in Eq. (6) of Tran and Dritschel[33](henceforth TD06). Before moving on the concrete calculations, we rewrite Eq. (C1). We symbolically express Eq. (C1) as

$$\frac{\mathrm{d}}{\mathrm{d}t}\hat{\psi} = \hat{N}. \tag{C2}$$

Here, N stands for the nonlinear term of the evolution equation. Multiplying (C2) by the complex conjugate of the modal stream function, $\hat{\psi}^*$, and then adding the resultant equation with their complex conjugate, we obtain

$$\frac{\mathrm{d}}{\mathrm{d}t}|\hat{\psi}|^2 = 2|\hat{\psi}|\frac{\mathrm{d}}{\mathrm{d}t}|\hat{\psi}| = \hat{\psi}^*\hat{N} + \hat{\psi}\hat{N}^*. \tag{C3}$$

If we express the Fourier component of a physical quantity A in terms of the amplitude and the phase as $\hat{A} = |\hat{A}|e^{i\theta_A}$, the last term of Eq. (C3) can be expressed as

$$\begin{aligned}\hat{\psi}^*\hat{N} + \hat{\psi}\hat{N}^* &= |\hat{\psi}||\hat{N}|\left\{\exp\left[i(\theta_N - \theta_\psi)\right] + \exp\left[i(\theta_\psi - \theta_N)\right]\right\} \\ &= 2|\hat{\psi}||\hat{N}|\cos\left[(\theta_N - \theta_\psi)\right].\end{aligned} \tag{C4}$$

Thus, the evolution equation for the absolute value of the modal stream function reduces to

$$\frac{\mathrm{d}}{\mathrm{d}t}|\hat{\psi}| = |\hat{N}|\cos(\theta_N - \theta_\psi) \leq |\hat{N}|. \tag{C5}$$

Noticing the fact that

$$\begin{aligned}|\hat{N}| &= \left|\sum_{\boldsymbol{l}}\sum_{\boldsymbol{m}} \delta_{\boldsymbol{k},\boldsymbol{l}+\boldsymbol{m}} \frac{l^\alpha - m^\alpha}{2k^\alpha} (\boldsymbol{m}\times\boldsymbol{l})_z \hat{\psi}(\boldsymbol{l})\hat{\psi}(\boldsymbol{m})\right| \\ &\leq \sum_{\boldsymbol{l}}\sum_{\boldsymbol{m}} \delta_{\boldsymbol{k},\boldsymbol{l}+\boldsymbol{m}} \left|\frac{l^\alpha - m^\alpha}{2k^\alpha} (\boldsymbol{m}\times\boldsymbol{l})_z\right| |\hat{\psi}(\boldsymbol{l})||\hat{\psi}(\boldsymbol{m})|,\end{aligned}$$

Eq. (C1) finally reduces to

$$\frac{\mathrm{d}}{\mathrm{d}t}|\hat{\psi}(\boldsymbol{k})| \leq \sum_{\boldsymbol{l}}\sum_{\boldsymbol{m}} \delta_{\boldsymbol{k},\boldsymbol{l}+\boldsymbol{m}} \left|\frac{l^\alpha - m^\alpha}{2k^\alpha} (\boldsymbol{m}\times\boldsymbol{l})_z\right| |\hat{\psi}(\boldsymbol{l})||\hat{\psi}(\boldsymbol{m})|. \tag{C6}$$

Next, we estimate the upper bound for $|(\boldsymbol{m}\times\boldsymbol{l})_z|$. Using the relation among the wave vectors in a triad,

$$\boldsymbol{k}=\boldsymbol{l}+\boldsymbol{m}, \tag{C7}$$

one obtains

$$\begin{aligned}(\boldsymbol{m}\times\boldsymbol{l})_z &= (\boldsymbol{m}\times\boldsymbol{k})_z = km\sin\theta_{km},\\ (\boldsymbol{m}\times\boldsymbol{l})_z &= (\boldsymbol{k}\times\boldsymbol{l})_z = kl\sin\theta_{kl},\end{aligned}$$

where θ_{km} is the angle between $\boldsymbol{k}$ and $\boldsymbol{m}$, and θ_{kl} is the angle between $\boldsymbol{k}$ and $\boldsymbol{l}$. The first and second equations yield

$$\begin{aligned}|(\boldsymbol{m}\times\boldsymbol{l})_z| &\le km,\\ |(\boldsymbol{m}\times\boldsymbol{l})_z| &\le kl,\end{aligned}$$

respectively. As a rigorous bound, one obtains

$$|(\boldsymbol{m}\times\boldsymbol{l})_z| \le k\min\{l,m\}. \tag{C8}$$

1. $\alpha = 3$ case

In the case of $\alpha=3$, Eq. (C6) is

$$\frac{\mathrm{d}}{\mathrm{d}t}|\hat{\psi}(\boldsymbol{k})| \le \sum_{\boldsymbol{l}}\sum_{\boldsymbol{m}}\delta_{\boldsymbol{k},\boldsymbol{l}+\boldsymbol{m}}\left|\frac{l^3-m^3}{2k^3}(\boldsymbol{m}\times\boldsymbol{l})_z\right||\hat{\psi}(\boldsymbol{l})||\hat{\psi}(\boldsymbol{m})|. \tag{C9}$$

We use the estimate Eq. (C8).

We derive the upper bound for $|l^3-m^3|$. In the case $l>m$, one obtains

$$\begin{aligned}\max\{|l^3-m^3|\} &= (\max\{l\})^3 - m^3\\ &= (m+k)^3 - m^3 = 3m^2k + 3mk^2 + k^3\\ &= 3km(k+m) + k^3 = 3klm + k^3.\end{aligned} \tag{C10}$$

In contrast, in the case $l<m$,

$$\begin{aligned}\max\{|l^3-m^3|\} &= (\max\{m\})^3 - l^3\\ &= (l+k)^3 - l^3 = 3l^2k + 3lk^2 + k^3,\\ &= 3kl(k+l) + k^3 = 3klm + k^3.\end{aligned} \tag{C11}$$

The above discussion yields

$$|l^3-m^3| \le 3kml + k^3. \tag{C12}$$

Even thought inserting Eq. (C12) into Eq. (C9), one cannot express the upper bound of $\frac{\mathrm{d}}{\mathrm{d}t}|\hat{\psi}(\boldsymbol{k})|$ in terms of $\mathcal{E}_3$ and k due to the existence of the second term on the right-hand side of Eq. (C12). In order to express it in terms of $\mathcal{E}_3$ and k, one must express the second term of Eq. (C12) by the first order term of k. If we assume that the wavenumbers of interest k exist in the infrared range, that is, we assume $k\le\min\{l,m\}$, k^3 is bounded as $k^3\le klm$. Then, Eq. (C12) is replaced by

$$|l^3-m^3| \le 4kml. \tag{C13}$$

However, because the summation in Eq. (C9) must be taken over the whole wavenumber range, there are wavenumbers l,m such that the condition $k\le\min\{l,m\}$ breaks down. Therefore, Eq. (C13) cannot be used in Eq. (C9). For the above reasons, the calculations by TD06 cannot be applied to the system with $\alpha=3$.

2. Arbitrary α case

We have pointed out that the discussion by TD06 fails in the application to the systems with $\alpha < 0$ and $\alpha = 3$. In this section, we point out that the similar problem appeared in the $\alpha = 3$ case arises when their calculations are applied to the system with $0 < \alpha < 3$.

In order to bound the time derivative of the modal stream function, we have to deduce the upper bound $|l^\alpha - m^\alpha|$. As similar to the previous discussion, for $l \le m$,

$$\begin{aligned} \max\{|l^\alpha - m^\alpha|\} &= (\max\{m\})^\alpha - l^\alpha \\ &= (l+k)^\alpha - l^\alpha. \end{aligned} \tag{C14}$$

Using the binomial expansion for $\alpha \in \mathbb{R}$,

$$\begin{aligned} (l+k)^\alpha &= l^\alpha (1 + k/l)^\alpha \\ &= l^\alpha \sum_{n=0}^{\infty} \binom{\alpha}{n} \left(\frac{k}{l}\right)^n \\ &= \sum_{n=0}^{\infty} \binom{\alpha}{n} l^{\alpha-n} k^n, \end{aligned} \tag{C15}$$

one obtains

$$\begin{aligned} (l+k)^\alpha - l^\alpha &= \sum_{n=1}^{\infty} \binom{\alpha}{n} l^{\alpha-n} k^n, \\ &= \binom{\alpha}{1} l^{\alpha-1} k + \binom{\alpha}{2} l^{\alpha-2} k^2 + \mathcal{O}\left(l^{\alpha-3} k^3\right) \\ &= \binom{\alpha}{1} l^{\alpha-2} k \left(l + \frac{\binom{\alpha}{2}}{\binom{\alpha}{1}} k \right) + \mathcal{O}\left(l^{\alpha-3} k^3\right) \\ &\le \binom{\alpha}{1} l^{\alpha-2} k m + \mathcal{O}\left(l^{\alpha-3} k^3\right). \end{aligned} \tag{C16}$$

Here, the binomial coefficient $\binom{\alpha}{n}$ is defined in terms of the gamma function as

$$\binom{\alpha}{n} = \frac{\Gamma(\alpha+1)}{\Gamma(n+1)\Gamma(\alpha-n+1)}. \tag{C17}$$

The ratio of the successive binomial coefficients is written as

$$\begin{aligned} \frac{\binom{\alpha}{n+1}}{\binom{\alpha}{n}} &= \frac{\Gamma(\alpha+1)}{\Gamma(n+2)\Gamma(\alpha-n)} \frac{\Gamma(n+1)\Gamma(\alpha-n+1)}{\Gamma(\alpha+1)} \\ &= \frac{\alpha-n}{n+1}. \end{aligned} \tag{C18}$$

Furthermore, the last step in Eq. (C16) has been obtained using

$$l + \frac{\alpha-1}{2} k \le l + k = m, \tag{C19}$$

because the physical relevance system must be $\alpha \le 3$.[9]

In the case α being a positive integer, the expansions (C15) and (C16) reduce finite series. However, when α is non-integer, the expansions (C15) and (C16) become infinite series. In order to converge the infinite series, the condition $k < l$ is required. This condition for convergence of the infinite series is the similar condition appeared in the case $\alpha = 3$. For those reasons, the calculations by TD06 cannot applied to the system except for $\alpha = 1$ and 2.

[1] N. Schorghofer, "Energy spectra of steady two-dimensional turbulent flows," Phys. Rev. E **61**, 6572 (2000).
[2] K. S. Smith, G. Boccaletti, C. C. Henning, I. Marinov, C. Y. Tam, I. M. Held, and G. K. Vallis, "Turbulent diffusion in the geostrophic inverse cascade," J. Fluid Mech. **469**, 13 (2002).
[3] C. V. Tran, "Nonlinear transfer and spectral distribution of energy in α turbulence," Physica D **191**, 137 (2004).
[4] T. Watanabe and T. Iwayama, "Unified scaling theory for local and non-local transfers in generalized two-dimensional turbulence," J. Phys. Soc. Jpn. **73**, 3319 (2004).
[5] T. Watanabe and T. Iwayama, "Interacting scales and triad enstrophy transfers in generalized two-dimensional turbulence," Phys. Rev. E **76**, 046303 (2007).
[6] E. Gkioulekas and K. K. Tung, "A new proof on net upscale energy cascade in two-dimensional and quasi-geostrophic turbulence," J. Fluid Mech. **576**, 173 (2007).
[7] J. Sukhatme and L. M. Smith, "Local and nonlocal dispersive turbulence," Phys. Fluids **21**, 056603 (2009).
[8] C. V. Tran, D. G. Dritschel, and R. K. Scott, "Effective degrees of nonlinearity in a family of generalized models of two-dimensional turbulence," Phys. Rev. E **81**, 016301 (2010).
[9] T. Iwayama and T. Watanabe, "Green's function for a generalized two-dimensional fluid," Phys. Rev. E **82**, 036307 (2010).
[10] K. Ohkitani, "Asymptotics and numerics of a family of two-dimensional generalized surface quasi-geostrophic equations," Phys. Fluids **24**, 095101 (2012).
[11] T. Iwayama, M. Sueyoshi, and T. Watanabe, "Linear stability analysis of parallel shear flows for an inviscid generalized two-dimensional fluid system," J. Phys. A: Math. Theor. **46**, 065501 (2013).
[12] B. H. Burgess and T. G. Shepherd, "Spectral nonlocality, absolute equilibria, and Kraichnan-Leith-Batchelor phenomenology in two-dimensional turbulent energy cascades," J. Fluid Mech. **725**, 332 (2013).
[13] R. T. Pierrehumbert, I. M. Held, and K. L. Swanson, "Spectra of local and nonlocal two dimensional turbulence," Chaos, Solitons Fractals **4**, 1111 (1994).
[14] T. Iwayama, T. G. Shepherd, and T. Watanabe, "An 'ideal' form of decaying two-dimensional turbulence," J. Fluid Mech. **456**, 183 (2002).
[15] I. M. Held, R. T. Pierrehumbert, S. T. Garner, and K. L. Swanson, "Surface quasi-geostrophic dynamics," J. Fluid Mech. **282**, 1 (1995).
[16] W. Blumen, "Uniform potential vorticity flow: Part I. Theory of wave interactions and two-dimensional turbulence," J. Atmos. Sci. **35**, 774 (1978).
[17] V. D. Larichev and J. C. McWilliams, "Weakly decaying turbulence in an equivalent-barotropic fluid," Phys. Fluids A **3**, 938 (1991).
[18] T. Watanabe, H. Fujisaka, and T. Iwayama, "Dynamical scaling law in the development of drift wave turbulence," Phys. Rev. E **55**, 5575 (1997).
[19] T. Watanabe, T. Iwayama, and H. Fujisaka, "Scaling law for coherent vortices in decaying drift rossby wave turbulence," Phys. Rev. E **57**, 1636 (1998).
[20] J. Pedlosky, *Geophysical Fluid Dynamics*, 2nd ed. (Springer–Verlag, 1987).
[21] R. H. Kraichnan, "Inertial ranges in two-dimensional turbulence," Phys. Fluids **10**, 1417 (1967).
[22] C. E. Leith, "Diffusion approximation for two-dimensional turbulence," Phys. Fluids **11**, 671 (1968).
[23] G. K. Batchelor, "Computation of the energy spectrum in homogeneous two-dimensional turbulence," Phys. Fluids **12**, II-233 (1969).
[24] C. Basdevant, M. Lesieur, and R. Sadourny, "Subgrid-scale modeling of enstrophy transfer in two-dimensional turbulence," J. Atmos. Sci. **35**, 1028 (1978).
[25] S. Yanase and M. Yamada, "The effect of the finite Rossby radius on two-dimensional isotropic turbulence," J. Phys. Soc. Jpn. **53**, 2513 (1984).
[26] T. Iwayama, T. Watanabe, and T. G. Shepherd, "Infrared dynamics of decaying two-dimensional turbulence governed by the Charney-Hasegawa-Mima equation," J. Phys. Soc. Jpn. **70**, 376 (2001).
[27] P. A. Davidson, "On the large-scale structure of homogeneous two-dimensional turbulence," J. Fluid Mech. **580**, 431 (2007).
[28] S. Fox and P. A. Davidson, "Integral invariants of two-dimensional and quasigeostrophic shallow-water turbulence," Phys. Fluids **20**, 075111 (2008).
[29] R. H. Kraichnan, "Eddy viscosity in two and three dimensions," J. Atmos. Sci. **33**, 1521 (1976).
[30] U. Frisch and P. L. Sulem, "Numerical simulation of the inverse cascade in two-dimensional turbulence," Phys. Fluids **27**, 1921 (1984).
[31] J. R. Chasnov, "On the decay of two-dimensional homogeneous turbulence," Phys. Fluids **9**, 171 (1997).
[32] S. Ossia and M. Lesieur, "Large-scale energy and pressure dynamics in decaying 2d incompressible isotropic turbulence," J. Turbul. **2**, N13 (2001).
[33] C. V. Tran and D. G. Dritschel, "Large-scale dynamics in two-dimensional Euler and surface quasigeostrophic flows," Phys. Fluids **18**, 121703 (2006).
[34] P. B. Rhines, "Waves and turbulence on a β-plane," J. Fluid Mech. **69**, 417 (1975).
[35] R. H. Kraichnan, "Inertial-range transfer in two- and three-dimensional turbulence," J. Fluid Mech. **47**, 525 (1971).
[36] M. Lesieur, *Turbulence in Fluids*, 4th ed. (Springer, 2008).
[37] C. Canuto, M. Y. Hussaini, A. Quarteroni, and T. A. Zang, *Spectral Methods in Fluid Dynamics* (Springer-Verlag, 1988).
[38] A. J. Lowe and P. A. Davidson, "The evolution of freely-decaying, isotropic, two-dimensional turbulence," Eur. J. Mech. B **24**, 314 (2005).
[39] C. Das, S. Kida, and S. Goto, "Overall self-similar decay of two-dimensional turbulence," J. Phys. Soc. Jpn. **70**, 966 (2001).